View metadata, citation and similar papers at core.ac.uk

brought to you by CORE

provided by K-State Research Exchange

METHODS FOR OPTIMIZATION OF THE SIGNATURE-BASED RADIATION SCANNING APPROACH FOR DETECTION OF NITROGEN-RICH EXPLOSIVES

by

KENNARD CALLENDER

B.S., University of New Orleans, 2002

M.S., University of Missouri-Rolla, 2007

AN ABSTRACT OF A DISSSERTATION

submitted in partial fulfillment of the

requirements for the degree

DOCTOR OF PHILOSOPHY

Department of Mechanical and Nuclear Engineering

College of Engineering

KANSAS STATE UNIVERSITY

Manhattan, Kansas

2015

ABSTRACT

The signature-based radiation scanning (SBRS) technique can be used to rapidly detect nitrogen-rich explosives at standoff distances. This technique uses a template-matching procedure that produces a figure-of-merit (FOM) whose value is used to distinguish between inert and explosive materials. The present study develops a tiered-filter implementation of the signature-based radiation scanning technique, which reduces the number of templates needed. This approach starts by calculating a normalized FOM between signatures from an unknown target and an explosive template through stages or tiers (nitrogen first, then oxygen, then carbon, and finally hydrogen). If the normalized FOM is greater than a specified cut-off value for any of the tiers, the target signatures are considered not to match that specific template and the process is repeated for the next explosive template until all of the relevant templates have been considered. If a target's signatures match all the tiers of a single template, then the target is assumed to contain an explosive. The tiered filter approach uses eight elements to construct artificial explosive-templates that have the function of representing explosives cluttered with real materials. The feasibility of the artificial template approach to systematically build a library of templates that successfully differentiates explosive targets from inert ones in the presence of clutter and under different geometric configurations was explored. In total, 10 different geometric configurations were simulated and analyzed using the MCNP5 code. For each configuration, 51 different inert materials were used as inert samples and as clutter in front of the explosive cyclonite (RDX). The geometric configurations consisted of different explosive volumes, clutter thicknesses, and distances of the clutter from the neutron source. Additionally, an objective function was developed to optimize the parameters that maximize the sensitivity and specificity of the method.

METHODS FOR OPTIMIZATION OF THE SIGNATURE-BASED RADIATION SCANNING APPROACH FOR DETECTION OF NITROGEN-RICH EXPLOSIVES

by

KENNARD CALLENDER

B.S., University of New Orleans, 2002

M.S., University of Missouri-Rolla, 2007

A DISSSERTATION

submitted in partial fulfillment of the

requirements for the degree

DOCTOR OF PHILOSOPHY

Department of Mechanical and Nuclear Engineering

College of Engineering

KANSAS STATE UNIVERSITY

Manhattan, Kansas

2015

Approved by:

Major Professor

Dr. William L. Dunn

ABSTRACT

The signature-based radiation scanning (SBRS) technique can be used to rapidly detect nitrogen-rich explosives at standoff distances. This technique uses a template-matching procedure that produces a figure-of-merit (FOM) whose value is used to distinguish between inert and explosive materials. The present study develops a tiered-filter implementation of the signature-based radiation scanning technique, which reduces the number of templates needed. This approach starts by calculating a normalized FOM between signatures from an unknown target and an explosive template through stages or tiers (nitrogen first, then oxygen, then carbon, and finally hydrogen). If the normalized FOM is greater than a specified cut-off value for any of the tiers, the target signatures are considered not to match that specific template and the process is repeated for the next explosive template until all of the relevant templates have been considered. If a target's signatures match all the tiers of a single template, then the target is assumed to contain an explosive. The tiered filter approach uses eight elements to construct artificial explosive-templates that have the function of representing explosives cluttered with real materials. The feasibility of the artificial template approach to systematically build a library of templates that successfully differentiates explosive targets from inert ones in the presence of clutter and under different geometric configurations was explored. In total, 10 different geometric configurations were simulated and analyzed using the MCNP5 code. For each configuration, 51 different inert materials were used as inert samples and as clutter in front of the explosive cyclonite (RDX). The geometric configurations consisted of different explosive volumes, clutter thicknesses, and distances of the clutter from the neutron source. Additionally, an objective function was developed to optimize the parameters that maximize the sensitivity and specificity of the method.

TABLE OF CONTENTS

CHAPTER 1 – INTRODUCTION

1.1 Research Background

Attacks from improvised explosive devices (IEDs) are one of the major threats to military and law enforcement personnel, as well as to civilians. To counter this threat, several technologies have been developed to detect IEDs. The existing technologies for explosive detection can be classified into three groups: non-explosive component detection, trace detection, and bulk detection.

Non-explosive component detection methods consist of detecting IED parts that are not explosive by nature, such as detonators, shell casings, and unique circuitry. These methods are not widely used because of their high rate of false alarms.

Trace-detection methods rely on detecting explosive vapors or particulates that can be sampled and identified. The main disadvantages of these techniques are that they require collection of vapor samples from the vicinity of the target or examination of the target at a short range.

Bulk detection methods attempt to identify macroscopic properties of the explosive device mainly through imaging or scanning methods. Imaging bulk-detection methods, such as computed tomography (CT) and radiography, have the drawbacks of relying on user interpretation (or complex software algorithms) and of not being well suited for standoff detection. Scanning bulk-detection methods, such as neutron interrogation techniques, have achieved some success. A good survey article is provided by Buffler [1].

The IED detection problem is very complicated, and improved methods are required. In particular, a system that can detect IEDs rapidly, from a safe distance, and that does not depend on user interpretation, is sought.

The signature-based radiation scanning (SBRS) method developed by Dunn et al. [2] has the potential to detect IEDs in a rapid (completed within seconds), remote (standoff distances of over a meter), and automated (no analysis of an image required) manner. This method uses characteristic back-streaming radiation responses (signatures) from unknown targets jointly with a template-matching procedure to recognize hidden explosives. Photon-scattered and photon-induced positron annihilation signatures [3] as well as inelastic-scatter and prompt-capture gamma ray signatures [4] have been used successfully in preliminary research to detect explosive surrogates. Radiation signatures such as these can be obtained from interrogating an unknown target and then can be compared to a library of known explosive templates. Each explosive template consists of radiation signatures expected for a given explosive in a particular configuration. A particular configuration is specified by several factors, such as the type, placement, and quantity of explosive, and the type, placement, and quantity of inert material (clutter) in relation to the explosive.

One of the main challenges of the SBRS technology is the need to develop a systematic method that reduces all the possible configurations of the explosive templates to a finite and manageable number. The response of an explosive sample is affected by several factors such as chemical composition, distance from the neutron source, quantity, nearby clutter material, and so forth. In order for the template matching procedure to work, these factors must be incorporated into the explosive templates in a systematic and efficient way. The more an explosive template resembles an explosive sample the easier it is to identify the explosive accurately. Therefore, the explosive template library should efficiently consist of as many explosive templates in different configurations as needed to be effective, with the constraint that the number of these templates should be manageable by a computer. The overall goal of this research is to develop a method

that will reduce the number of explosive templates necessary to distinguish between unknown explosive and inert samples under several different conditions, including the presence of clutter. Achieving this goal involves investigation of a tiered-filter approach and construction of an objective function whose maximum identifies the optimum model parameters.

1.2 Statement of the Problem

This study addresses the problem of differentiating an unknown target that contains a nitrogen-rich explosive sample (an IED), from a target that contains only non-explosive materials. The technique must be able to provide a systematic method of constructing a library of templates that identifies most explosive samples of all the possible different target configurations subject to the constraints that exist in the field (e.g., the space constraint that an explosive configuration is subject to an interrogated volume within the trunk of a car) and that discards inert samples. In particular, the technique must be able to use a finite and manageable number of templates to identify explosive samples that have clutter thicknesses, distance from the source, and explosive volumes that are slightly different from those characteristic of the library templates. Additionally, the technique must also provide a robust method to represent the infinite types of possible clutter material by a finite number of templates. The approach is to develop a tiered-filter technique, based on the SBRS technology.

1.3 Research Objectives

The main goal of this study is to develop a technique based on the signature-based radiation scanning method that identifies targets that contain nitrogen-rich explosives at standoff distances of greater than 0.5 m with high levels of sensitivity and specificity. The specific objectives are:

- Develop a method that is able to identify an explosive sample even in the presence of clutter in different geometric configurations. The following configuration parameters are

considered in this study:

  - Clutter chemical composition
  - Clutter thickness
  - Distance of clutter from neutron source
  - Explosive volume

- Focus on incorporating features into the method that exploit particular characteristics of nitrogen-rich explosives to differentiate them from inert materials.
- Identify the limitations of the method for each particular type of configuration.
- Develop a systematic methodology of constructing a library of templates that identifies explosive samples of all the possible different target configurations. In essence, the method should be able to identify a large number of explosive configurations with a relatively small number of templates.
- Define a normalized form of the figure-of-merit function.
- Construct an algorithm that optimizes the parameters used in the method to give the best performance based on sensitivity and specificity.

1.4 Significance of the Study

Improvised explosive devices have been used in conflicts throughout the world since World War II. However, the threat of these devices has increased since the second conflict in Iraq. Due to the high number of deaths and injuries from IEDs, the United States Army put together a special task force in the fall 2004 to find solutions to reduce the threat from IEDs [5]. The effort and large investment made by the United States Army to solve this problem, indicates the seriousness of the IED threat.

The feasibility to use the signature-based radiation scanning method to detect IEDs has

been established. The SBRS technology has the ability to be simple, rapid, automated, and remote. The library of templates in the SBRS method plays a crucial role in identifying explosives of different target configurations. The method presented in this study, provides a systematic approach to build this library of templates. If successful, IEDs in different target configurations, which include the presence of clutter, can be identified with high levels of sensitivity and specificity.

1.5 Definition of Terms

This section provides definitions for terms with which the reader might not be familiar. In addition, common terms that have a special meaning in the study are presented.

Explosive – In this study, explosives refers exclusively to nitrogen-rich explosives [6].

Inert – In this study, inert refers to any material that is not a nitrogen rich explosive. Thus, even though some materials can be dangerous (e.g., anthrax, nitrogen rich fertilizers), they are not considered explosives.

Clutter – Any inert material that alters the response of the detection system.

True Positive – A reading from the system indicating that an explosive is present, when an explosive is in fact present.

True Negative – A reading from the system indicating that no explosive is present, when no explosive is in fact present.

True Suspect – A reading from the system indicating that the presence of an explosive is suspected, when an explosive is in fact present.

False Positive - A reading from the system indicating that an explosive is present, when no explosive is in fact present.

False Negative - A reading from the system indicating that no explosive is present, when an

explosive is in fact present.

False Suspect – A reading from the system indicating that the presence of an explosive is suspected, when an explosive is in fact not present.

Remote – Ideally, a safe distance so that the detection system is not severely harmed if the explosive device detonates. However, because this research is in its preliminary stages, it refers to distances 0.5 m or larger.

Sensitivity – Performance indicator that reflects the ability of a system to identify an explosive if an explosive is present. In this study, the mathematical definition of sensitivity is modified to include samples labeled as suspects.

Specificity – Performance indicator that reflects the ability of a system to identify an inert if an inert is present. In this study, the mathematical definition of specificity is modified to include samples labeled as suspects.

Target – A volume interrogated by the detection system that may or may not contain an explosive sample hidden inside it.

Signature – A characteristic response from a target that can be used to differentiate explosive targets from inert ones.

1.6 Organization of the Study

Existing and potential standoff explosive detection techniques are reviewed in Chapter 2. A historical overview of the problem and a description of the elements of detection are given in the first sections. The chemical composition and density of nitrogen rich explosives is also considered. These characteristics of nitrogen rich explosives are very important because the method presented in this study relies heavily on them. Trace and bulk detection methods are the two main types of detection techniques that are reviewed. The signature-based radiation

scanning technique is reviewed in Section 2.6. This technique provides the basis for the method developed in this research.

The tiered-filter approach to the signature-based radiation scanning technique is introduced in Chapter 3. The theoretical background is given in section 3.3. Then the method is described and its potential to achieve the objectives described in section 1.3 is discussed. Section 3.5, presents the procedure through which the parameters used by the tiered-filter approach are optimized. The objective function that maximizes the sensitivity and specificity is discussed in this section.

The experimental procedure is discussed in Chapter 4. Simulation results based on MCNP5 were performed. The geometry used for the simulations is presented in Section 4.3. Section 4.4 describes how the explosive and inert samples were generated. Section 4.5 describes how the library of artificial templates is built. This section is of great importance because it addresses one of the main objectives of this research.

The experimental results produced by the tiered-filter approach are given in Chapter 5. Different cases testing the performance of the method are presented. This is done by calculating the sensitivity and specificity produced by libraries of artificial templates and the sets of unknown samples that have clutter composition, clutter thickness, distance from the source, or explosive volumes different from the templates in the libraries. Results using the tiered-filter approach are compared against the original signature-based radiation scanning figure-of-merit.

A summary of the study is presented in Chapter 6. Conclusions and discussion of the experimental results obtained in Chapter 5 are presented here. Recommendation for future research is given in the final section.

CHAPTER 2 – REVIEW OF SELECTED LITERATURE AND RESEARCH

2.1 Chapter Overview

This chapter reviews the literature and research related to this study. First, a brief overview of the history of the IED problem is given. The major conflicts where this device has been used in large scales are presented here. Then, the concepts that describe the IED problem, the methodologies to assess the performance of explosive detection systems, and the parameters that describe the explosive devices and their environment, are discussed. The typical chemical composition and density of nitrogen-rich explosives are presented in section 2.4, among other important characteristics. Next, the literature of different explosive detection techniques is reviewed. The review is divided into trace detection and bulk detection methods. Finally, a literature review of the signature-based radiation scanning technique is given.

2.2 Brief Historical Overview of the Problem

The British Army was the first to come up with the term Improvised Explosive Devices (IEDs) in the 1970s to describe the highly effective booby trap devices or remote-controlled bombs, made from agricultural fertilizer and semtex, which were used by the Provisional Irish Republican Army (IRA). However, large scale use of IEDs occurred earlier, during World War II. In particular, the Belarussian guerrillas used command-detonated and delayed-fuse IEDs to derail German trains between 1943 and 1944 [7]. Improvised explosive devices have been extensively used since then in many conflicts, primarily in terrorist actions or unconventional warfare by guerrilla forces.

During the Vietnam War, the Viet Cong used IEDs against American land- and river-borne vehicles and personnel. The devices were usually built from unexploded ordnance from the American military forces. Thirty-three percent of American casualties during this conflict

were attributed to mines and IEDs [8].

The Provisional Irish Republican Army used IEDs extensively in Northern Ireland during 1969-1997. The IEDs developed by the IRA became highly sophisticated, featuring anti-handling devices such as mercury tilt switch or micro-switches that would detonate the explosive if moved in any way. The ongoing battle to gain the upper hand in electronic warfare with remote controlled devices led the bomb disposal teams from the 321 EOD (Explosive Ordnance Disposal) to employ specialists from QinetiQ, the Royal Signals, and Military Intelligence. Most of the modern techniques, weapons, and equipment currently used by EOD operators throughout the world resulted from this multi-unit approach [9].

The United States supplied the Afghan Mujahideen large quantities of military supplies six months before the USSR invasion of Afghanistan in 1979. The Afghan insurgents removed explosives from anti-tank mines and combined them in tin cooking oil cans for a more powerful blast. After these IEDs were detonated the Afghan insurgents often followed the attack with direct-fire weapons. Since the invasion of Afghanistan in 2001, the most common and dangerous method of attack against NATO forces, Afghan military, and civilian vehicles has been the use of IEDs. The attacks using these destructive devices has increased consistently [10].

In the Iraq 2003-2011 War, the damage that IEDs attacks had on American military forces was major. According to the Washington Post, 64% of U.S. deaths in Iraq were caused by IEDs [11]. Most of these devices were made with artillery or mortar shells, or with varying amounts of bulk or homemade explosives. The United Kingdom government charged that Iran was supplying insurgents with the technological know-how to build these IEDs [12]. This charge was denied by both the Iranian and Iraqi government officials [13].

Other conflicts that have seen extensive use of these destructive devices during unconventional guerrilla warfare or terrorist attacks are:

- Hezbollah used IEDs extensively against Israeli Forces after Israel's invasion of Lebanon in 1982 [14].
- The IEDs used by Chechnyan rebels during the First Chechnyan War (1994-1996) and the Second Chechnyan War (1999-2008) accounted for many Russian deaths [15].
- On July 13 of 2011, the Indian Mujahideen terrorist group detonated three IEDs on the city of Mumbai which killed 19 people and injured 130 more [16].
- Buses, trucks, and tanks were the target of IEDs used by military insurgents in the recent Syrian uprisings [17].

Because of the vast experience that military forces from Canada, India, Israel, Spain, United Kingdom, and the United States have had with IEDs used against them in either conflict or terrorists attacks, they are at the forefront of counter-IED efforts. However, because IEDs are improvised devices, there are no specific guidelines for explosive ordnance disposal (EOD) personnel to identify or categorize them. Currently, no comprehensive solution to the IED problem exists [18].

2.3 Elements of Detection: Concepts, Threats, and Devices

The process of detecting an explosive at a standoff distance involves receiving a signal, processing the signal, analyzing the results, and evaluating whether the target contains an explosive or not. The performance of detection methodologies are usually assessed by concepts such as the sensitivity and specificity of the system, or by the Receiver Operating Characteristic (ROC) curves. The definitions of sensitivity and specificity are given in section 1.5. The ROC curves are plots of the probability that a methodology will yield a true positive versus the

probability that the same methodology will yield a false positive. Consequently, ROC curves combine the sensitivity and specificity performance of a system, and provide a practical method of comparing different detection techniques. In this thesis, the objective function used to optimize the parameters of the tiered-filter approach (which also combines the sensitivity and specificity performance of the system) is used to evaluate the performance of the method instead of the ROC curves.

The overall performance of a detection system built on multiple technologies, in the presence of environmental, threat, and other potential detection confusers the system might face, is given by the system effectiveness (SE). The system effectiveness measures the scale to which a detection system achieves a set of specific mission requirements. It depends on the threat characterization, environment, and technology, among other factors. Furthermore, the concept of SE incorporates additional important concerns such as the mass of the explosive, available sampling time, and human intervention.

An essential component for solving the standoff bomb detection problem involves having a general understanding of the scenarios of concern, and the parameters that describe the explosive device and the surrounding environment. Two of the scenarios that are currently been given primary consideration because of the difficulty to detect them on time are suicide bombers and wide-area surveillance of explosives. The parameters that define these types of scenarios are known as threat parameters. These threat parameters can be categorized into three groups: those related to the local environment, those describing the explosive device, and those that characterize the bomber. From the parameters related to the local environment, the most important is the intended target of the explosive detonation. The reason for this is that an understanding of what the potential target might be, helps prioritize the areas that should be

monitored and protected.

Finally, a significant concept used to describe the relation between two or more explosive detection systems is the concept of orthogonality. If two detection methods are designed to detect independent characteristics of an IED then the methods are said to be orthogonal. When two or more of these orthogonal methods are used together they are referred to as a system of orthogonal detection technologies. The benefits of using such a system are that the sensitivity of the combined system is higher than that of the individual components, the effectiveness is also greater, and the difficulty of defeating the detection system increases.

2.4 Chemical Composition and Density of Explosives

Because of the diversity of potential explosive formulations, the detection of explosives based on their chemical characteristics represents a significant challenge. The problem of standoff bomb detection, however, narrows the focus to high explosives. Fortunately, if elemental formulations are considered, few common chemicals can be confused with nitrogen-rich high explosives. According to the online Aldrich catalog of common laboratory and industrial chemicals and polymers, which contains over 90,000 chemicals, only one explosive elemental composition from the 26 nitrogen-rich high explosives listed in Table 2.1 had an isomer. The explosive is TNT, which has the same elemental composition as dinitroanthranilic acid. Table 2.1 presents a list of nitrogen-rich high explosives that can easily be used as IEDs.

Table 2.1 Representative Common Nitrogen-Rich High Explosives and Their Compositions

Explosives Based on Nitrogen	Formula	wt % H	wt % C	wt % N	wt % O	Sum N+O
Ammonium Nitrate	$H_4N_2O_3$	5.04	0	35.01	59.97	94.98
Ammonium Picrate	$C_6H_6N_4O_7$	2.46	29.28	22.76	45.5	68.26
Cyclonite (RDX)	$C_3H_6N_6O_6$	2.72	16.22	37.84	43.22	81.06
Ethylenediamine Dinitrate	$C_2H_{10}N_4O_6$	5.42	12.91	30.1	51.58	81.68
Guanidine Nitrate	$CH_6N_4O_3$	4.95	9.84	45.89	39.32	85.21
Hexamethylenetriperoxide Diamine	$C_6H_{12}N_2O_6$	5.81	34.62	13.46	46.11	59.57
Hexanitrohexaazaisowurtzitane	$C_6H_6N_{12}O_{12}$	1.38	16.13	38.36	43.82	82.18
Hydrazine Nitrate	$H_5N_3O_3$	5.3	0	44.2	50.09	94.29
Mannitol Hexanitrate	$C_6H_8N_6O_{18}$	1.78	15.94	18.59	63.69	82.28
Monomethylene Nitrate	$CH_4N_2O_3$	4.38	13.05	30.43	52.14	82.57
Nitrocellulose	$C_6H_7N_3O_{11}$	2.37	24.24	14.14	59.23	73.37
Nitroglycerin	$C_3H_5N_3O_9$	2.22	15.87	18.5	63.41	81.91
Nitrotriazolone	$C_2H_2N_4O_3$	1.55	18.47	43.08	36.9	79.98
Octogen (HMX)	$C_4H_8N_8O_8$	2.72	16.22	37.84	43.22	81.06
Pentaerythritol Tetranitrate	$C_5H_8N_4O_{12}$	2.55	19	17.72	60.73	78.45
Picric Acid	$C_6H_3N_3O_7$	1.32	31.46	18.34	48.88	67.22
Tetrazene	$C_2H_8N_{10}O$	4.29	12.77	74.44	8.5	82.94
Tetryl	$C_7H_5N_5O_8$	1.76	29.28	24.39	44.58	68.97
Trinitrobenzene	$C_6H_3N_3O_6$	1.42	33.82	19.72	45.05	64.77
Trinitrotoluene	$C_7H_5N_3O_6$	2.22	37.02	18.5	42.26	60.76
Triminoguanidine Nitrate	$CH_9N_7O_3$	5.43	7.19	58.67	28.72	87.39
Triaminotrinitrobenzene	$C_6H_6N_6O_6$	2.34	27.92	32.55	37.19	69.74
Trinitroazetidine	$C_3H_4N_4O_6$	2.1	18.76	29.17	49.98	79.15
Trinitrochlorobenzene	$C_6H_2N_3O_6$	0.81	29.11	16.97	38.78	55.75
Trinitropyridine	$C_5H_2N_4O_6$	0.94	28.05	26.17	44.84	71.01
Urea Nitrate	$CH_5N_3O_4$	4.09	9.76	34.14	52	86.14
Average (%)		2.98	20.29	30.81	46.14	76.95
Standard Deviation		±1.38	±8.15	±11.01	±8.01	±8.47
Maximum/Minimum (%)		5/0.8	37/0	58/13	63/9	95/56

High explosives are composed of oxidizing and reducing agents, which can be in a single molecule such as TNT, nitroglycerin, or PETN, or within an ionic solid, such as ammonium nitrate when mixed with fuel oil. Strong oxidizing agents require the most electronegative elements such as nitrogen, oxygen, fluorine, and chlorine. Because of their difficult chemistry, instability, and greater expense, fluorine and chlorine are used significantly less often in high explosives. Therefore, typical high explosive chemicals contain large concentrations of nitrogen

and oxygen. Carbon and hydrogen serve as reductant components of high explosives. Sometimes metal powders such as aluminum or magnesium are also added as supplemental reducing agents. The density of these explosives typically ranges between 1.2 and 1.8 g/cm^3 [19].

The list of nitrogen explosives in Table 2.1 shows that the average nitrogen content is 30.81 ±11.01% and that the average oxygen content is 46.18±8.01%. These characteristics suggest that focus on percentage composition of nitrogen and oxygen might be a useful identifier of high explosives. It has been stated that "A measurement of the oxygen and nitrogen densities, to an uncertainty of ±20%, gives a unique separation of explosives from other compounds" [20]. Therefore, dual analysis of the nitrogen and oxygen concentration in a target provides more reliable identification of nitrogen-rich high explosives.

2.5 Standoff Explosive Detection Techniques

2.5.1 Trace Detection Methods

Trace detection methods attempt to detect explosive vapors or explosive particulates. Explosive vapors are gas molecules emitted from an explosive when the atmospheric pressure is greater than the vapor pressure of the explosive. Explosive particulates are microscopic particles that adhere to any surface that has been in direct or indirect contact with an explosive. Even though trace detection at standoff distances is a challenging task, several trace detection techniques have been developed and perform satisfactorily in certain scenarios. The three main types of trace detection methods are electronic/chemical, optical, and biosensor.

Two of the main electronic/chemical trace detection methods are chemiluminescence and mass spectrometry. Chemiluminescence uses chemical reactions that produce electromagnetic radiation in the form of ultraviolet, visible, and infrared light [21]. In particular, this method is

used to detect nitrogen-rich explosives by detecting infrared light produced from the reaction between nitric oxide and ozone [22]. Mass spectrometry detects residual traces of explosives in contamination of air, dust, and so forth. The method analyzes a substance in relation to the mass of its corresponding atoms, and it can be based on time separation or geometric separation [23].

Optical methods include infrared spectroscopy and microcantilevers. Infrared spectroscopy is used to identify the chemical composition of explosives by examining the absorption spectrum from explosive particulates and vapors [24]. Microcantilevers detection consists of detecting explosive particulates using a cantilever. Molecules absorbed on the unsupported side of the cantilever causes bending which can be monitored with high sensitivity [25]. Some of the benefits of this method for detection include the miniature size of the cantilevers, array detection capabilities, high sensitivity, and low power consumption [26].

Biosensors use the sense of smell or olfaction to detect explosives. Canines, pigs, rats, bees, and microorganisms can be used as biosensors [27]. In particular, canines are frequently used, because of their exceptional olfactory ability and because they can be easily trained [28]. The disadvantages of these methods include expensive training, brief operation time, and limited life-time of the animal.

2.5.2 Bulk Detection Methods

Bulk detection methods attempt to recognize macroscopic properties of the explosive. These methods implement photon, microwave, or neutron techniques to identify the shape, density, or composition of the explosive. The advantages of bulk detection methods compared to several trace detection methods are greater sensitivity, specificity, penetrability, as well as being able to operate at standoff distances and being able to interrogate the target faster.

X-ray transmission technology provides information about the target density. It is very

advanced and is used in many airport screening scenarios [29]. Unfortunately, this method is ill-suited for standoff detection. Backscattered X rays can be used at standoff distances [29]. However, the low levels of specificity and the inability to effectively overcome explosive shielding present significant difficulties for this technology. Computed tomography allows two-dimensional images to be constructed, which provides excellent spatial resolution. Different types of computed tomography are direct X-ray transmission imaging, coded X-ray scatter imaging, and coherent scatter X-ray computed tomography [30]. These methods are ill-suited for standoff detection because of the extensive scanning around the target.

Electromagnetic imaging methods include microwave scanning and nuclear quadrupole resonance. Microwave scanning can operate at standoff distances of 1 m or greater and requires simple inexpensive equipment [31]. Millimeter wave methods are similar to microwaves for detection purposes [32]. Both of these methods are best suited to interrogate people because they can penetrate clothing but have difficulties penetrating thicker clutter materials. Nuclear quadrupole resonance is based on magnetic resonance physics. It consists of applying a specific electric field gradient, which flips the nuclei electric quadrupole moment, generating a nuclear quadrupole resonance pulse [33]. This method has been used to detect explosives such as RDX, PETN, and HMX [34]. However, because it has to be within close range of the target, it is not well suited for standoff detection.

Two advantages of neutron interrogation techniques over the methods mentioned earlier are the ability to identify the stoichiometric composition of explosives and the capability to penetrate tens of cm into low and high Z materials. Neutron methods can use thermal neutrons (thermal neutron analysis), fast neutrons (fast neutron analysis and pulsed fast neutron analysis), or both (pulsed fast and thermal neutron analysis). The benefit of thermal neutron analysis is

that the absorption cross section for thermal neutrons is much higher than that for fast neutrons [1][35][36]. However, portable intense sources of thermal neutrons are difficult to manufacture. In fast neutron analysis, inelastic-scatter gamma rays are detected by high energy resolution detectors, such as high purity germanium detectors [35][36]. Pulsed fast neutron analysis is similar to fast neutron analysis, but neutrons are emitted in multiple nanosecond pulses [36]. Pulsed fast and thermal neutron analysis consists of interrogating a target by alternating pulsed fast and thermal neutron beams [37].

2.6 Signature-Based Radiation Scanning Technique

The Signature-Based Radiation Scanning (SBRS) technique is a radiation interrogation method developed by Dunn et al [2] that can be used to detect IEDs in a fast, standoff, and automated manner. This method uses characteristic back-streaming radiation responses, called signatures, from unknown samples in combination with a template-matching procedure to evaluate if the target contains an explosive. It has been shown that the technique is capable of detecting explosive surrogates by using photon-scattered and photon-induced positron annihilation signatures [3] as well as inelastic-scatter and prompt-capture gamma ray signatures [4]. After interrogating an unknown target the signatures are collected by detectors and then be compared to signatures in a library of known explosive templates. The templates in the library contain signatures obtained for a given explosive in a particular configuration. Different factors, such as the type, placement, and quantity of explosive, and the type, placement, and quantity of inert material (clutter) in relation to the explosive, specify these configurations.

CHAPTER 3 – TIERED-FILTER APPROACH TO THE SIGNATURE-BASED RADIATION SCANNING TECHNIQUE

3.1 Chapter Overview

This chapter presents the proposed method to solve the IED problem as stated in Section 1.2. The method is called the tiered-filter approach (TFA) to the SBRS technique, which is based on the SBRS technique developed by Dunn et al [2]. Optimization of the parameters used in the TFA is also described in this chapter.

First a brief literature review and the theoretical background of the method are presented. The theoretical background includes a review of nuclear physics and of the SBRS technique. Then the TFA method, with all its different components and its benefits, is described. The components that have been developed in this research are:

- Hydrogen, Carbon, Nitrogen, and Oxygen (HCNO) tiers.
- Density tier.
- Artificial templates.
- Normalization of figure-of-merit function.

These components and their benefits are described in Section 3.4.

Finally, the optimization of the parameters used in the TFA approach is described. This is achieved by maximizing an objective function that portrays the performance of the system after having labeled (correctly or incorrectly) unknown targets in a group as explosives or non-explosives. The optimization of the objective function utilizes a simulated annealing algorithm. Construction and optimization of the objective function is a contribution of this research. The simulated annealing algorithm was taken from *Numerical Recipes in FORTRAN 77*.

3.2 Review of Selected Literature and Research

The detection of improvised explosive devices (IEDs) at standoff distances is a very complicated and daunting challenge. A number of technologies have been developed to address this problem. These can be classified into three main groups: non-explosive component detection, trace detection, and bulk detection. In particular, scanning bulk-detection methods, such as neutron interrogation techniques, have achieved some success. A survey article is provided by Buffler [1]. In spite of this, systems with better performance are still required.

A radiation interrogation method that has the potential to detect IEDs in a rapid, remote, and automated manner, is the signature-based radiation scanning (SBRS) technique developed by Dunn et al [2]. Characteristic back-streaming radiation responses, called signatures, from unknown samples are used jointly with a template-matching procedure to identify hidden explosives. Preliminary research has shown that the method is able to detect explosive surrogates by using photon-scattered and photon-induced positron annihilation signatures [3] as well as inelastic-scatter and prompt-capture gamma ray signatures [4]. Signatures such as these can be collected by detectors after interrogating an unknown target and then can be compared to a library of known explosive templates. Each explosive template in the library contains the responses obtained for a given explosive or an explosive-like substance in a particular configuration. These configurations are specified by different factors, such as the type, placement, and quantity of explosive, and the type, placement, and quantity of inert material (clutter) in relation to the explosive.

3.3 Theoretical Background

3.3.1 Elements of Nuclear Physics

Atoms are composed of a nucleus surrounded by a cloud of electrons. The nucleus is composed of protons and neutrons. The number of protons in the nucleus determines the element. Therefore, interaction with the nucleus can give information about what element is present (stoichiometry). Beams of neutrons and gamma rays combined with gamma detectors and neutron detectors can be used to obtain valuable information about the stoichiometry and density of explosives.

Neutrons have neutral charge and interact primarily with nuclei, not with electrons. Nuclear forces that occur between neutrons and nuclei act at close range; therefore neutrons must pass near nuclei to interact with them. Because the size of the nucleus is much smaller than the size of the atom, neutrons can penetrate significantly into matter.

As neutrons penetrate through matter, two types of scattering may occur. Elastic scattering occurs when the nucleus is left in the ground state, while inelastic scattering occurs when the nucleus is left in an excited state. In both cases, the scattered neutron has less kinetic energy than the incident neutron by the amount of recoil and excitation energy (if any) of the scattered nucleus. The process of a neutron losing energy through scattering until it becomes in thermal equilibrium is denoted neutron thermalization. The maximum energy loss occurs when the size of a nucleus is similar to that of a neutron. Because of this, hydrogen is the most efficient moderator of neutrons.

As neutrons thermalize, the probability that they undergo radiative capture increases. The radiative capture (n, γ) reaction consists of a nucleus absorbing a neutron, forming a compound nucleus in an excited state, which then decays to the ground state by gamma-ray

emission. These gamma photons generally decay promptly (less than 10^{-6} s) and thus are known as prompt capture gamma rays. These gamma rays have energies characteristic of the isotope, making it possible to identify what isotope is emitting them.

Inelastic scattering also provides the means of identifying isotopes. The inelastic scattering (*n, n'*) reaction occurs when a nucleus scatters a neutron, but leaves the nucleus in an excited state, which then decays to the ground state by gamma-ray emissions. The inelastic gamma rays emitted have energies that are characteristic of the struck isotope and thus can be used to identify the isotope from which they were emitted.

3.3.2. Signature-Based Radiation Scanning

The feasibility of using the signature-based radiation scanning (SBRS) method to rapidly detect chemical explosives at standoff distances has been demonstrated by Dunn et al. [2]. The SBRS method consists of active interrogation of a target by neutron and/or photon radiation beams, which leads to a set of responses or signatures collected by detectors on the same side of the target as the source. Significantly more information about the target is obtained when both neutron and photon radiation beams are used. Therefore combined use of these two is preferred. The set of responses collected by the detectors can then be used in a template-matching procedure, which provides a figure-of-merit (FOM) to distinguish between inert and explosive materials.

The signatures from an unknown target collected by the detectors are used to construct a response vector $\boldsymbol{U}$ of J components, where J is the number of signatures used. This response vector $\boldsymbol{U}$ is then compared to a library of templates, one by one. Each template, $\boldsymbol{K_t}$, in the library is a vector of J signatures from an explosive sample in a particular configuration. Here $\boldsymbol{t} = 1, 2, \ldots, T$ where T is the total number of specified configurations of an explosive target. Neutron

generated gamma signatures correspond to the net number of counts under a peak from a prompt-capture or inelastic-scatter gamma ray. Backscatter photon signatures correspond to detector response spectra integrated between two energies. Bare and cadmium covered neutron detectors can also provide two additional signatures that are dependent on the density and composition of the contents of the target. If the vector ***U*** matches at least one of the explosive templates in the library to a sufficient degree, then it is presumed that the unknown target is an explosive. Otherwise, it is inferred that the unknown target contains only inert materials.

The template-matching procedure consists of using a chi-square-like figure-of-merit of the form [3]:

$$\zeta_t = \sum_{j=1}^{J} \alpha_j \frac{\left(\beta U_j - K_{tj}\right)^2}{\beta^2 \sigma^2\left(U_j\right) + \sigma^2\left(K_{tj}\right)}, \tag{3.1}$$

where U_j is the jth measured signature of an unknown sample, K_{tj} is the jth signature for the tth template, J is the number of signatures, β is a factor that scales the measured values to the template values, σ^2 is the variance, and α_j is a normalized weight factor given by

$$\alpha_j = \frac{\omega_j}{\sum_{j=1}^{J} \omega_j}, \tag{3.2}$$

with ω_j being a positive weight for the jth signature. Equation (3.2) implies

$$\sum_{j=1}^{J} \alpha_j = 1. \tag{3.3}$$

An estimate of the standard deviation of the FOM has been derived from the widely used propagation of errors formula [4]. The propagation of errors formula, for a function f of two variables a and b, is given by

$$\sigma^2(f)=\left|\frac{\partial f}{\partial a}\right|^2\sigma^2(a)+\left|\frac{\partial f}{\partial b}\right|^2\sigma^2(b)+2\frac{\partial f}{\partial a}\frac{\partial f}{\partial b}\mathrm{cov}(ab), \tag{3.4}$$

where $\sigma^2(a)$ and $\sigma^2(b)$ are the variances of the variables a and b, respectively, and cov(ab) is the covariance between this variables. If the variables are independent of each other then the covariance is zero.

It can be shown (see Appendix A) that the covariance terms between the variables U_j, K_{tj}, $\sigma^2(U_j)$, and $\sigma^2(K_{tj})$ are zero. Thus, the standard deviation of the figure of merit of Eq. (3.1) can be written as

$$\sigma(\zeta_t)=\left\{\sum_{j=1}^{J}\left[\frac{\partial\zeta_t}{\partial U_j}\right]^2\sigma^2(U_j)+\sum_{j=1}^{J}\left[\frac{\partial\zeta_t}{\partial K_{tj}}\right]^2\sigma^2(K_{tj})\right.$$
$$\left.+\sum_{j=1}^{J}\left[\frac{\partial\zeta_t}{\partial\sigma^2(U_j)}\right]^2\sigma^2(\sigma^2(U_j))+\sum_{j=1}^{J}\left[\frac{\partial\zeta_t}{\partial\sigma^2(K_{tj})}\right]^2\sigma^2(\sigma^2(K_{tj}))\right\}^{1/2}. \tag{3.5}$$

The terms $\sigma^2(\sigma^2(U_j))$ and $\sigma^2(\sigma^2(K_{tj}))$ are known as the variance of the variance (VOV). The partial derivatives in Eq. (3.5) are given by

$$\frac{\partial\zeta}{\partial U_j}=\frac{2\alpha_j\beta(\beta U_j-K_{tj})}{\beta^2\sigma^2(U_j)+\sigma^2(K_{tj})}, \tag{3.6}$$

$$\frac{\partial\zeta}{\partial K_{tj}}=\frac{-2\alpha_j(\beta U_j-K_{tj})}{\beta^2\sigma^2(U_j)+\sigma^2(K_{tj})}, \tag{3.7}$$

$$\frac{\partial\zeta}{\partial\sigma^2(U_j)}=\frac{-\alpha_j\beta^2(\beta U_j-K_{tj})^2}{\left[\beta^2\sigma^2(U_j)+\sigma^2(K_{tj})\right]^2}, \tag{3.8}$$

and

$$\frac{\partial\zeta}{\partial\sigma^2(K_{tj})}=\frac{-\alpha_j(\beta U_j-K_{tj})^2}{\left[\beta^2\sigma^2(U_j)+\sigma^2(K_{tj})\right]^2}. \tag{3.9}$$

A first approximation to the standard deviation of the FOM is obtained by neglecting the VOV terms. Substituting Eq. (3.6) and Eq. (3.7) into Eq. (3.5), and neglecting the VOV terms gives

$$\sigma(\zeta_t)=\left\{\sum_{j=1}^{J}\left[\frac{2\alpha_j(\beta U_j-K_{tj})}{\beta^2\sigma^2(U_j)+\sigma^2(K_{tj})}\right]^2\left[\beta^2\sigma^2(U_j)+\sigma^2(K_{tj})\right]\right\}^{1/2}. \tag{3.10}$$

After simplifying, the final form of Eq. (3.10) is given by

$$\sigma(\zeta_t)=2\left[\sum_{j=1}^{J}\alpha_j^2\frac{(\beta U_j-K_{tj})^2}{(\beta^2\sigma^2(U_j)+\sigma^2(K_{tj}))}\right]^{1/2}. \tag{3.11}$$

A second, and more accurate, approximation to the standard deviation of the FOM that does not neglect the VOV terms, has also been developed, and is derived in Appendix B. The first approximation, however, is the one that has been used in the SBRS formulation [3][4].

An additional feature of the original SBRS formulation [3][4], is that the FOM and the standard deviation are used to define filter functions

$$f_{\pm}(\lambda)=\zeta_t\pm\lambda\sigma(\zeta_t), \tag{3.12}$$

where λ is a constant that can be adjusted to specify the "confidence-like" interval. If $f_{-}(\lambda) > f_o$ for all templates in the library, where f_o is a specified cut-off value, then the target is deemed an inert. Similarly, if $f_{+}(\lambda) < f_o$ for at least one template in the library, then the target is deemed an explosive. If neither test is true, the result is inconclusive, and the target is considered a suspect. The values of the parameters λ and f_o are established by the user to adjust for sensitivity and specificity. Filter functions, however, are not used for the tiered-filter approach. The process of determining if a target is an explosive or not in the tiered-filter approach is explained in section 3.4.1.

The advantages of the SBRS technique over other IED detection methods include the following:

- Rapid detection of IEDs due to a simplified process that focuses only on determining the presence of an explosive and not the complete stoichiometry of the contents of the target.
- The system contains components that can be operated at remote (standoff) distances and the operator can be at a safe remote location.
- Human interpretation is seldom required. Perhaps the only exception to this is when the FOM is very near the cut-off value. In such cases, additional evaluation of the target by a trained operator might be required.

3.4 Tiered-Filter Approach

3.4.1 Basic Description of the Method

One of the most difficult challenges the SBRS technology faces is the need of a systematic method to build a library of explosive templates that successfully differentiates explosive and inert samples from among all the possible different target configurations subject to the constraints that exist in the field. The size of the trunk of a car is an example of a constraint to which an explosive configuration is subject. The response vector of an explosive sample is influenced by several factors. In order for the template matching procedure to be successful, these factors must be incorporated into the explosive templates methodically. The more an explosive template resembles a particular explosive sample configuration, the lower the FOM value should be. The infinite number of possible configurations requires a systematic method to reduce the number of explosive templates necessary to distinguish between inert and explosive materials to a finite and manageable number.

The tiered-filter approach is a modified version of the template-matching procedure described in the section 3.3.2. This approach facilitates the construction of a library of templates

by exploiting the particular characteristics of nitrogen-rich explosives (i.e., the substantially higher concentration of nitrogen and oxygen, as well as higher density of explosives compared to other inert materials containing HCNO elements). The tiered-filter approach consists of calculating FOM values between an unknown sample and an explosive template through stages, evaluating if the sample has the appropriate concentration of each element (nitrogen first, then oxygen, then carbon, and finally hydrogen) to contain an explosive. If a sample fails at least one of these stages (ζ for that stage greater than ζ_N , ζ_O , ζ_C , or ζ_H, where ζ_X is the cutoff value for element *X*), it is discarded (for that specific template), and the process is repeated for the next explosive template in the library until all of the explosive templates have been considered. If a sample passes through all the tiers of a single template (ζ for the tier smaller than ζ_N , ζ_O , ζ_C , or ζ_H), then it is considered an explosive.

The current study uses only prompt-gamma or inelastic-gamma ray signatures from hydrogen, carbon, nitrogen, and oxygen. However, backscatter photon signatures, as well as signatures from bare and cadmium-covered neutron detectors can be easily incorporated.

3.4.2 Density Tier

One problem that the tiered-filter approach has is the difficulty of distinguishing inert samples with a low density but with very similar chemical compositions to explosives (i.e., high concentration of N and O, and low concentration of C and H), from explosive samples that have a high density clutter in front of them. This is because the response collected by the detectors from these explosive samples is reduced due to the high density clutter (usually metals with density higher than 3 g/cm^3). Additional information about the clutter density can prove to be very valuable in reducing the number of false positives in the system and improving the results in general. Some photon interrogation methods have the capability to estimate the average density

of the target.

The density tier is a preliminary tier that classifies explosive templates in the library according to their average density. By incorporating this tier into the system, the average density of an unknown target can then be evaluated and compared only to the templates that belong to the same range that it does. Better results can be achieved in this way, because only the explosive templates that have average densities similar to the unknown sample are used to calculate the FOM value.

3.4.3 Artificial Templates

The tiered filter approach uses artificial templates, which are constructed for targets that contain a real or characteristic explosive sample with artificial inert materials (clutter). The artificial inert materials have the function of representing all the different real inert materials that can occur in the field. The concentration of nitrogen, oxygen, carbon, and hydrogen in the clutter material changes the proportion of the (HCNO) response detected from the explosive sample. Therefore, the artificial inert materials in the artificial templates consist of different combinations of HCNO, and a filler element. The filler element has the function of taking the place of the elements that are not HCNO. The types of atoms affect the response, so filler elements representing different ranges of atom types should be used. Other factors that affect the response collected by the detectors are the clutter density, the clutter thickness and the explosive thickness. Discrete values are used to represent the range of densities of different real inert materials, and the range of thicknesses of clutter and explosive (sample configurations) that can occur in the field.

Artificial templates, $\boldsymbol{K_t}$, are vectors of signatures representing different explosive configurations. Each artificial template is divided into four sets of responses. Each set consists

of the signatures corresponding to the elements H, C, N, and O. The response vector ***U*** is also divided into four sets corresponding to each element. Each signature is the net number of counts under a peak from a prompt-capture or inelastic-scatter gamma ray. If a set of signatures from the response vector matches the corresponding set for a particular artificial template to a sufficient degree, then the process is repeated for the next set of signatures (tier). The nitrogen (N) tier is evaluated first, then the oxygen (O) tier, then the carbon (C) tier, and finally the hydrogen (H) tier. If the signature vector from an unknown sample passes all the tiers then the unknown is considered an explosive. If there fails to be a match at any stage (tier) of the process, then it is presumed that the response vector for the unknown does not match that particular artificial template to a sufficient degree, and the process is repeated for the next artificial template in the library.

3.4.4 Normalized Figure-of-Merit Function

A normalized version of the FOM function is used at every tier to evaluate if a set of signatures from the response vector and the artificial template matches to a sufficient degree. The normalized FOM is defined by

$$\zeta_t = \frac{\sum_{j=1}^{J} \alpha_j \frac{\left(U_j - K_{tj}\right)^2}{\sigma^2\left(U_j\right) + \sigma^2\left(K_{tj}\right)}}{\sum_{j=1}^{J} \alpha_j \frac{K_{tj}^{\ 2}}{\sigma^2\left(K_{tj}\right)}}. \tag{3.13}$$

Thus if the net number of counts under every peak of the response vector for a particular set of signatures (tier) is zero, then the FOM value equals one. If there is a perfect match between the response vector and the artificial template, then the FOM value is zero. One benefit of using Eq. (3.13) is that only four cut-off values (one for each tier) are required for all the templates in the

library instead of requiring different cut-off values for each template. The cut-off values are given by ζ_N, ζ_O, ζ_C, and ζ_H, which correspond to the Nitrogen, Oxygen, Carbon, and Hydrogen tiers, respectively. A second benefit is that the percent that an unknown sample matches the explosive template can be known.

The standard deviation of Eq. (3.13) is given by

$$\sigma(\zeta_t) = \frac{2\left[\sum_{j=1}^{J} \alpha_j^2 \frac{(U_j - K_{tj})^2}{(\sigma^2(U_j) + \sigma^2(K_{tj}))}\right]^{1/2}}{\sum_{j=1}^{J} \alpha_j^2 \frac{K_{tj}^{\ 2}}{\sigma^2(K_{tj})}}. \tag{3.7}$$

3.4.5 Benefits of the Tiered-Filter Approach

The tiered-filter approach is based on the SBRS technique, and because of this, the benefits of the latter system are inherent to the former one. These benefits were mentioned at the end of section 3.3.2. However, the tiered-filter approach offers additional advantages that make the system more robust for the field. In summary, the benefits of the tiered-filter approach include the following:

- Enables the construction of a library of templates by using artificial templates to represent a broad range of possible explosive configurations subject to the constraints imposed by the field.
- Fewer templates are required because the chemical composition of any clutter material can be represented by a relatively small number of elements (HCNO, and filler elements).
- Exploits the fact that explosive samples contain a significantly higher concentration of nitrogen than most other inert materials. This prevents the effects from nitrogen (N) signatures to be "washed-off" by other signatures.

- The density tier reduces the number of false positives and improves the system in general by comparing unknown samples only to explosive templates that have average densities similar to them.
- Cut-off values can be set individually for each tier, instead of having just one cut-off value for the whole template. If a cut-off value is set too high, the probability that an inert sample is deemed an explosive or a suspect increases. Therefore, having cut-off values for each tier gives greater flexibility in keeping them as low as required by the signatures of each element (H, C, N, and O) and thus minimizes the number of false positives.
- Inert samples are discarded without evaluating the complete template, thus making search faster.

3.5 Optimization of Parameters in Tiered-Filter Approach

3.5.1 Sensitivity and Specificity Functions

A key objective of this study is to calculate the parameters in the TFA that give the best results. The fundamental probabilistic and statistical elements of assessing performance of standoff bomb detection methods are sensitivity and specificity. One reasonable solution of obtaining the parameters that offer the best results is to develop an objective function that is defined in terms of the sensitivity and specificity of the system. However, the traditional definitions of these terms are not completely well suited for the TFA method, and they need to be redefined. First the basic definitions are reviewed, then the reason for modifying them is given, and finally the new formulations for sensitivity and specificity are presented.

To start, suppose an experimenter has an IED detection system with a binary output (indicating if the target contains an explosive or not), and the experimenter can verify if an

explosive is indeed present or not. If the experimenter runs a number of tests, and records the output from the detection system and the true status of the test, then a table can be made reflecting the four possible outcomes. Table 3.1 illustrates the possible combinations that can occur.

Table 3.1 Detector Output vs. True Status of Test for IED Detection Systems

	Explosive Was Present	No Explosive Was Present
Detector Indicated Explosive was Present	True Positive (L_E)	False Positive (M_I)
Detector Indicated No Explosive was Present	False Negative (M_E)	True Negative (L_I)
	Total Number of Explosive Targets (N_E)	Total Number of Non-Explosive Targets (N_I)

In Table 3.1, L_E stands for explosives that were correctly labeled as explosives (True Positives), L_I stands for inerts that were correctly labeled as inerts (True Negatives), M_E stands for missed explosives or explosives that were incorrectly labeled as inerts (False Negatives), and M_I stands for missed inerts or inerts that were incorrectly labeled as explosives (False Positives). The total number of explosive targets and non-explosive targets are represented by N_E and N_I respectively.

As can be deduced from Table 3.1, the sum of True Positives (L_E) and False Negatives (M_E) equals the total number of explosive targets. Similarly, the sum of False Positives (M_I) and True Negatives (L_I) equal the total number of non-explosive targets. The traditional mathematical definition of sensitivity and specificity are given by

$$Sensitivity = \varepsilon_n = \frac{L_E}{L_E + M_E} = \frac{L_E}{N_E}, \quad \text{and} \tag{3.8}$$

$$Specificity = \varepsilon_p = \frac{L_I}{L_I + M_I} = \frac{L_I}{N_I} = \frac{N_I - M_I}{N_I} \quad . \tag{3.9}$$

3.5.2 Objective Function

The objective function that has been defined in this study to evaluate the performance of the method is given by

$$\Omega = \omega_n \varepsilon_n + \omega_p \varepsilon_p \tag{3.10}$$

$$\text{with} \quad \omega_n + \omega_p = 1,$$

where ω_n and ω_p are weight factors specified by the user to give more value in the optimization process to the sensitivity or the specificity, respectively. Combining equations 3.8, 3.9, and 3.10 gives

$$\Omega = \omega_n \left[\frac{L_E}{N_E} \right] + (1 - \omega_n) \left[1 - \frac{M_I}{N_I} \right]. \tag{3.11}$$

As can be seen, this objective function depends on the number of true positives, false positives, number of explosives and number of inerts. The first two variables, in turn, depend on the cut-off values for the different tiers and the weight factors for the different signatures. Therefore, the objective function Ω is a multidimensional function that cannot be simply optimized.

3.5.3 Simulated Annealing Algorithm based on Downhill Simplex Method

An important component of the present research is to determine the values of the parameters that give the best performance of the tiered-filter approach technique, and the method through which these values were obtained. The basic statistical and probabilistic elements of assessing

performance of standoff bomb detection methodologies are given by the sensitivity and specificity of the method. Because of this, an objective function that is a function of the sensitivity and specificity was defined, and a suitable optimization method was chosen. The goal is to find the values of the parameters that maximize this function. It should be noted however, that because the given methods in the book *Numerical Recipes in Fortran 77* are minimizing algorithms, the negative form of the objective function was evaluated in the codes for convenience. The objective function was defined in section 3.5.2.

Because of the normalization condition of Eq. (3.3), there are only five independent weight factors, four for nitrogen and one for oxygen. Thus, the objective function of Eq. (3.11) is actually a function of ten independent variables, ω_n , ζ_N , ζ_O , ζ_C , ζ_H , α_{N1}, α_{N2}, α_{N3}, α_{N4}, α_{O1}. Even though the partial derivatives of the objective function with respect to L_E, and M_I exist and are continuous; the partial derivatives with respect to the independent variables may not be continuous. Therefore, a multidimensional optimization method that does not require the computation of first derivatives is sought. The optimization method that has been selected in this research is a combination of simulated annealing and the downhill simplex method. Generally speaking, simulated annealing is the fundamental method being used, and it's goal is to find the global minimum of the objective function. The downhill simplex method has the function of increasing the efficiency of converging to a local minimum. Both methods will now be described. First, the downhill simplex method, then the simulated annealing method, and finally the combined versions of the two, are presented.

3.5.3.1 Downhill Simplex Method

The downhill simplex method is a multidimensional minimization method that requires evaluations only of functions, not derivatives. It was developed by Nelder and Mead [38].

Unlike most optimization methods, the downhill simplex method does not make explicit use of one-dimensional optimization algorithms as a part of its computational strategy. Instead it uses a geometrical figure called a simplex to move through *N*-dimensional space in search of the smallest (optimal) value.

A simplex is a geometrical figure in *N*-dimensional space consisting of *N + 1* vertices and their interconnected line segments. For example, in two-dimensional space, a simplex is a triangle; in three-dimensional space it is a tetrahedron; etc. Only non-degenerate simplexes are used in the downhill simplex method (i.e; simplexes that enclose a finite inner *N*-dimensional volume). The *N + 1* vertices in the simplex are given by

$$\vec{P}_i = \vec{P}_o + \lambda \vec{e}_i \quad , \quad i = 1, 2, ..., N,$$

where P_o is the initial starting point selected by the user (any point), e_i's are *N* unit vectors, λ is a constant that is the users' estimate of the characteristic length, and P_i are the rest of the points in the simplex.

The downhill simplex method consists of making the vertices in the simplex move through the complex *N*-dimensional topography of the independent variables, evaluating the objective function at the vertices, and moving downhill, until it encounters values of the independent variables that give at least a local minimum of the objective function.

There are four types of movement that the vertices follow. These are reflection, reflection and expansion, contraction, and multiple-contraction. These movements depend on the position of three particular points of the simplex, which are:

- Highest point (vertex of the simplex where the function is the highest)
- Next highest point (vertex of the simplex where the function is the second highest)

- Lowest point (vertex of the simplex where the function is the lowest)

The goal of the movements is to find points smaller than the highest points and next highest points and replace them. The first movement a simplex performs is a reflection (or mirror image) of the highest point through the other *N* points of the simplex. If the reflected point is smaller than the lowest point, then an expansion (extrapolation) along the line of reflection is made to perhaps find an even smaller point. If the reflected point is larger than the second highest point, then a contraction along the line of reflection is made. If this last point is still higher than the previous higher value, then movement along that line doesn't seem to improve the situation, and a multiple contraction around the lowest value is then performed.

In essence, the points that are evaluated first are the ones along the line of reflection of the original highest point. If there is no improvement along this line (through reflection, and contraction), then a multiple contraction around the lowest point is performed, and the process is repeated again. If there is an improvement along this line (through reflection) then an expansion is performed and the process is repeated again. This algorithm will converge to a local minimum when the difference between the high point and the low point of the simplex is smaller than a tolerance value provided by the user.

3.5.3.2 Simulated Annealing

Simulated annealing is a multidimensional minimization technique that is suitable for large scale problems, and that has the advantage of not getting easily stuck in local minima. It requires only function evaluations, no derivatives. It is particularly powerful for combinatorial optimization, and has effectively solved the famous *traveling salesman problem* [39].

The method resembles the process of annealing, where at high temperatures the molecules of a metal move freely with respect to one another. If cooling occurs slowly, thermal

mobility is lost, atoms are often able to align themselves, and the system reaches a state of minimum energy. If quick cooling or "quenching" occurs the system ends up in a higher energy state. So the analogy is that while other optimization methods go greedily downhill (quick cooling) and can get stuck in a local minimum; simulated annealing incorporates a mechanism that, once in a while, allows it to get out of local minima (slow cooling) and encounter better results, increasing the chances of ending up at the global minimum. The use of the simulated annealing algorithm, however, does not guarantee a global minimum will be reached.

Metropolis [40] was the first to develop an algorithm based on the concept of annealing. The method consists of offering a succession of energy options to a simulated thermodynamic system. The system will change its configuration from an energy state E_1 to an energy state E_2 with a probability of

$$p = \exp\left[-(E_2 - E_1)/kT\right]$$

where k (Boltzman constant) is a constant of nature that relates energy to temperature and T is the temperature of the system.

In the case when $E_2 < E_1$, the probability is larger than one. In such a case the probability is arbitrarily set equal to one, and as a result of this, the system always takes the smaller configuration (E_2). This is the mechanism that allows the simulated algorithm of always taking a downhill step while still having a chance of taking uphill steps from time to time. If $E_2 > E_1$, then $0 < p < 1$ and an uphill step is taken. This uphill step gives the method a chance of getting out from a local minimum. As the iterations continue, the temperature of the system decreases according to an annealing schedule. A reduction in the parameter T reduces the probability of an uphill step, and eventually (if the reduction of the temperature is slow enough) the system will converge to a good local minimum.

The main ideas of the Metropolis algorithm are also applicable to optimization process of continuous variables, and the four components required for the algorithm are the following:

- An objective function $f(\boldsymbol{x})$, where $\boldsymbol{x}$ is an N-dimensional vector of the N independent variables. This function is the analog of the energy of the system, whose minimization is the goal of the procedure.
- Possible system configurations. The different system configurations are represented by the function $f(\boldsymbol{x})$ evaluated at different values $\boldsymbol{x}$.
- A generator of random changes in the configuration. Which means there must be a procedure for taking a random step from $\boldsymbol{x}$ to $\boldsymbol{x}+\boldsymbol{\Delta x}$.
- A control parameter $\boldsymbol{T}$ (analog of temperature) and an annealing schedule. The annealing schedule tells how often and by how much the parameter $\boldsymbol{T}$ must be lowered. For example, the parameter $\boldsymbol{T}$ can be held constant for $100N$ reconfigurations, or for $10N$ successful reconfigurations, whichever comes first. Once this occurs, the parameter $\boldsymbol{T}$ is decreased, and the process is repeated until efforts to reduce the objective function become discouraging.

The objective function, its variables, and the annealing schedule are specified by the user (with some trial and error being the most difficult part in deciding the most efficient annealing schedule). However, the generator of random changes in the configuration does present a significant problem. A key factor of the Metropolis simulated annealing algorithm, is that the mechanism generally takes a step downhill in the optimization process, while sometimes taking a step uphill. For that reason, an internal mechanism that always takes a downhill step in an efficient way, while sometimes taking an uphill one is required.

3.5.3.3 Combined Methodology

The approach taken in by the authors of *Numerical Recipes in Fortran 77* is to modify the downhill simplex method so that it generally takes a downhill step, while sometimes taking a step uphill. This is done by adding random numbers proportional to the annealing temperature (thermal fluctuations) to the current function value at the vertices of the simplex (current energy state, E_1). Random numbers proportional to the annealing temperature are then subtracted from the function value at the new proposed vertix of the simplex (new energy state, E_2). In this way, if the original value of the new energy state (E_2) is smaller than the current energy state (E_1), then subtracting a positive random number from E_2, while adding a positive random number to E_1, would still leave E_2 smaller than E_1. As a result, a downhill step would generally be taken. However, if the original value of E_2 is larger than E_1, then because of the subtracting and adding of positive random numbers to E_2 and E_1, respectively, there is a chance that the modified value of E_2 would emerge smaller than the modified value of E_1. Consequently, there is a chance that an uphill step is taken. The chance of an uphill step decreases proportionally to the annealing temperature, which in turn decreases according to an annealing schedule specified by the user.

CHAPTER 4 - SIMULATION PROCEDURE

4.1 Chapter Overview

In this study, computer simulations, instead of real experiments, were used to test the tiered-filter implementation of the SBRS method. This Chapter discusses reasons why computer simulations were utilized, and explains the procedure employed to produce the data necessary to evaluate the performance of the method. The Chapter starts by describing the code used to run the computer simulations. It gives a brief description of how the MCNP code works and why the results produced by it can be trusted. It also talks about how the data were post-processed. Then the geometry of the simulation is described. All the important components of the simulation, as well as the different configurations are portrayed. The section that follows identifies the explosive and inert samples that were used. The method through which the artificial explosive templates were made, including their compositions and densities, is discussed in the final section.

4.2 MCNP Code for Simulation

The code used in this study to test the feasibility of the tiered-filter approach was the Monte Carlo N-Particle (MCNP) code. MCNP is a particle transport code developed and maintained at Los Alamos National Laboratory. It is an internationally recognized code for analyzing the transport of neutrons, gamma rays, electrons, and coupled particles, including secondary gamma rays resulting from neutron interactions. The code undergoes continuous development at Los Alamos National Laboratory, and new versions are released periodically. The version used in this study is MCNP5.

MCNP employs the Monte Carlo methodology to perform simulations of different particles. In essence, the Monte Carlo method is a highly flexible and powerful numerical integration technique that uses sample means to estimate population means. A wide variety of

direct and inverse problems can be solved using this methodology. These problems can be posed as numerical quadratures (problems formulated as integrals) or as simulations (problems where the integral formulation is not specified). The method is based on two powerful mathematical theorems, which are the strong law of large numbers and the central limit theorem. These theorems are used to obtain an estimate of an expected value (strong law of large numbers) and the corresponding uncertainty of the estimate (the central limit theorem). Therefore, Monte Carlo simulation provides an estimate of what the answer to the problem is, and how good that estimate is.

In order to simulate an experiment in MCNP the user creates an input file. This file contains all the necessary information to run the simulation. The input file consists of the title card, cell cards, surface cards, and data cards. The term card, historically a punch card, refers to a code line in the input file. Additionally, the cell cards, surface cards, and data cards are also referred to as Block 1, Block 2, and Block 3, respectively. The title card consists of only one line with the title given to the simulation by the user. The cell cards (Block 1) together with the surface cards (Block 2) have the function of specifying the geometry of the problem. The data cards (Block 3) provide all the other problem specifications other than the geometry. These include the materials used, type of particles, radiation sources, cross section libraries, how results are tallied, and so forth.

The use of powerful computers to perform the simulation enables MCNP to run a large number of particle histories, and thus provide a very precise answer. The accuracy of the nuclear physics theory and the cross sectional data incorporated into the MCNP code has been thoroughly tested by professional experts at Los Alamos National Laboratory and elsewhere. The code has been used to design nuclear reactors and other complex systems. Therefore, the

accuracy and the precision of the results from the simulations obtained by running the MCNP code can be trusted, if enough histories are run, to test feasibility of the tiered-filter approach to the SBRS technique.

Running computer simulations instead of real-life experiments has the purpose of testing the feasibility of a method in a much more economical, safe, and fast manner. If a method proves to be feasible, then more expensive real-life experiments can be performed to test it under field conditions. Because this study is in the early stages of testing the feasibility of the tiered-filter approach, computer simulations based in MCNP5 are appropriate.

4.3 Simulation Geometry

Ten different types of target geometric configurations were simulated and analyzed using the MCNP5 code. The different configurations try to isolate the effects of the clutter chemical composition, clutter thickness, position of the explosive and clutter, and explosive volume. For each geometric configuration, 102 samples were generated. Half of the targets consisted of an explosive cyclonite (RDX) sample with 51 different clutter materials in front of it, and the other half consisted only of the same inert material as both the sample and the clutter.

All the targets were inside a thin aluminum box. The aluminum box has the function of hiding the contents. It was 0.2 cm thick and the dimensions were of 1 m on each side. For all cases, the clutter material had a width of 96 cm and a height of 20 cm, and the explosive had a width of 15.24 cm and a height of 20 cm. A neutron beam, aligned with the clutter and the explosive sample, was placed 50 cm in front of the aluminum box. The energy of the neutrons was 14.1 MeV (representative of a collimated D-T neutron generator), and the number of source particle histories was 2×10^{7}. A point detector was placed 35 cm directly above the neutron beam. The width of the energy bins for the tally was 4-keV. This width was selected to

resemble the energy resolution of some HPGe detectors. A total of nine prompt-gamma and inelastic-gamma ray signatures from hydrogen, carbon, nitrogen, and oxygen were used in the simulations. The signatures used in this study are shown in Appendix E. The simulations assumed the source, detector, and target were all in a vacuum. Figure 4.1 shows schematically a side view of the simulation setup. The different types of configuration are described in Table 4.1. The different values used for the clutter thickness, the explosive thickness, and the distance from the neutron source to the clutter are given by the variables t_c , t_e and d_s, respectively.

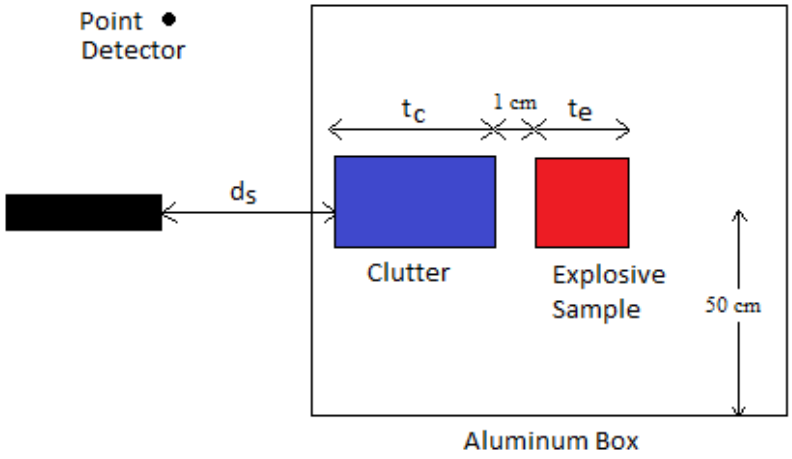

Figure 4.1. Schematic of the experimental setup (side view). The sample contained either the explosive cyclonite (RDX) or the same material as the clutter material. The target is bombarded by a neutron beam, and the response is collected by a point detector.

Table 4.1 Distance from the Source, Clutter thickness, and Explosive Thickness for the Different Geometric Configurations Simulated in this Study

Configurations	Distance from Source d_s (cm)	Clutter Thickness t_c (cm)	Explosive Thickness t_e (cm)
Configuration 1	74	10	11
Configuration 2	69	15	11
Configuration 3	64	20	11
Configuration 4	59	25	11
Configuration 5	54	30	11
Configuration 6	69	10	16
Configuration 7	64	10	21
Configuration 8	59	10	26
Configuration 9	64	10	11
Configuration 10	54	10	11

4.4 Explosive and Inert Samples

A wide range of inert materials were selected to test the feasibility of the method. These materials where used as clutter in front of the explosive cyclonite, and each material was also used as clutter and sample. Table 4.2 shows the 51 different materials that were used as clutter and as inert samples.

Table 4.2 List of Materials Used as Clutter and as Inert Samples

1	Air	18	Gasoline	35	Polyurethane
2	Aluminum	19	Glass	36	Propane
3	Antifreeze	20	Granite	37	Rubber
4	Ash	21	Herbicide 1	38	Salt
5	Borax	22	Herbicide 2	39	Soap
6	Bricks	23	Herbicide 3	40	Soil
7	Carbon	24	K Hydroxide	41	Soy
8	Cardboard	25	Lead	42	Steel
9	Ceramic	26	Limestone	43	Styrofoam
10	Cherrywood	27	Lucite	44	Sugar
11	Concrete	28	Nickel	45	Tissue
12	Copper	29	Nylon	46	Titanium
13	Cotton	30	Petroleum	47	Void
14	Cyanurate	31	Plexiglass	48	Water
15	Ethanol	32	Polyethylene	49	Wax
16	Fertilizer A	33	Polypropylene	50	Woodoak
17	Fertilizer B	34	Polystyrene	51	Zirconium

4.5 Explosive Artificial Templates

4.5.1 Chemical Composition

Artificial templates were generated for each configuration. These templates assumed a cyclonite explosive sample with artificial inert material in front of it. The artificial inert materials in front of the explosive consist of different possible combinations of HCNO, and a filler element. The filler element has the function of taking the place of the elements that are not HCNO. Section 4.5.2 gives more details about the function of filler elements in the construction of artificial material.

Artificial materials have the function of representing all the different real inert materials that can occur in the field. The discrete values that were used to represent the concentration of the different elements were all multiples of 10%. Whenever the sum of the concentrations of H, C, N, and O did not add up to a 100% a filler element was used. Table 4.3 shows the chemical composition of the artificial templates that required a filler element. Similarly, Table 4.4 shows the chemical composition of the artificial templates that did not require a filler element. The combinations chosen in these Tables are the values that are closest to the HCNO concentration of the inert materials in Table 4.2. It should be noted that the artificial inert materials should not resemble explosives; therefore they only contain a maximum of 20% nitrogen at lower densities, and none for higher densities (densities greater than 3 g/cm^3).

4.5.2 Filler Elements and Density

The filler element used in generating artificial materials has the function of taking the place of the elements that are not HCNO. The filler materials used were selected by trial and error among elements that did not have interference gammas. Elements with properties that would have offered difficulty (such as the high neutron absorption rate of boron) were discarded. Lithium (Li), fluorine (F), phosphorus (P), and chromium (Cr), were used as filler elements. A higher clutter density implied a higher probability that an interaction will occur with the clutter elements and the smaller the chance they will interact with the explosive. This means that the density of the material also affects the response of the target; therefore discrete values were used to represent them. Densities of 0.25 g/cm^3 (Very Low Density), 1 g/cm^3 (Low Density), 2.25 g/cm^3 (Medium Density), and 7 g/cm^3 (High Density) were used to represent the range of densities of the different real inert materials.

In order to produce artificial templates that resemble real inert materials well, only the combinations among filler elements and densities shown in Table 4.5 and Table 4.6 were used. This was done to avoid having unrealistic materials that possess, for example, a very light element with a very high density. Additionally, the artificial templates were divided into lower density templates (Table 4.5) and higher density templates (Table 4.6), which enables the use of a preliminary density tier, such that unknown samples are compared only with the templates that correspond to a particular density range.

Table 4.3 Chemical Composition of Artificial Explosive Samples with their Filler Element

	Nitrogen	Oxygen	Carbon	Hydrogen	Filler Element
1	0%	0%	0%	0%	100%
2	0%	0%	30%	60%	10%
3	0%	10%	30%	50%	10%
4	0%	20%	0%	0%	80%
5	0%	20%	20%	50%	10%
6	0%	30%	0%	30%	40%
7	0%	40%	0%	50%	10%
8	0%	40%	10%	0%	50%
9	0%	50%	0%	0%	50%
10	0%	60%	0%	0%	40%
11	0%	60%	20%	0%	20%
12	0%	70%	0%	0%	30%

Table 4.4 Chemical Composition of Artificial Explosive Samples without Filler Element

	Nitrogen	Oxygen	Carbon	Hydrogen
1	0%	0%	100%	0%
2	0%	0%	30%	70%
3	0%	0%	40%	60%
4	0%	0%	50%	50%
5	0%	10%	20%	70%
6	0%	10%	30%	60%
7	0%	20%	20%	60%
8	0%	20%	30%	50%
9	0%	20%	40%	40%
10	0%	30%	0%	70%
11	0%	80%	10%	10%
12	10%	0%	30%	60%
13	10%	0%	40%	50%
14	10%	10%	30%	50%
15	10%	10%	40%	40%
16	10%	10%	50%	30%
17	20%	0%	30%	50%

Table 4.5 Filler Elements and their Corresponding Densities

For the Lower Density Tier

Density	Value (g/cm^3)	Range (g/cm^3)	Filler element
Very Low Density	0.25	0 – 0.5	Li
Very Low Density	0.25	0 – 0.5	F
Low Density	1.0	0.5 – 1.5	Li
Low Density	1.0	0.5 – 1.5	F
Low Density	1.0	0.5 – 1.5	P
Medium Density	2.25	1.5 – 3.0	F

Table 4.6 Filler Elements and their Corresponding Densities

For the Higher Density Tier

Density	Value (g/cm^3)	Range (g/cm^3)	Filler Element
Medium Density	2.25	1.5 – 3.0	Cr
High Density	7.0	3.0 – 11.0	P
High Density	7.0	3.0 – 11.0	Cr

CHAPTER 5 – EXPERIMENTAL RESULTS

5.1 Chapter Overview

In this chapter, the results obtained by applying the tiered-filter approach described in Chapter 3 to the MCNP simulations discussed in Chapter 4 are presented. The performance of the tiered-filter approach is evaluated by using the objective function defined in section 3.5.2. The sensitivity and the specificity of the method are also calculated. In all sections, the results are also obtained without using the HCNO tiers. For ease of reference, these results are labeled non-tiered approach. This was done to observe if the use of tiers does indeed improve the performance of the system compared to the non-tiered method. The results shown in this Chapter are discussed in Chapter 6.

The first section discusses the library of explosive templates used in all the results shown. The library consists of 126 normalized templates, of which three are applied to high density targets (densities above 3 g/cm^3) and the rest are applied to lower density targets. All the templates in the library were constructed from the same geometric configuration, which is labeled as the default configuration. The next section shows the materials used as clutter in front of the sample, either the explosive cyclonite or inert materials. A total of 51 different materials are included.

Section 5.3 shows the results obtained by applying the library of templates to inert and explosive samples that have the same geometric configuration as the templates in the library. The goal of this section was to see how effectively the artificial materials (clutter) used in the explosive templates work when applied to the real materials employed in the explosive and inert targets, everything else been equal.

The next three sections try to isolate the effects of changing the position of the target,

increasing the explosive volume, and increasing the clutter thickness, respectively. The templates in the library (which were developed for the default configuration) are applied to targets of different geometric configurations. This is done to see how well the templates in the tiered-filter approach handle targets that have slightly different geometric configurations, and to estimate the limitations in how well they work.

The last section applies the library of templates to all the target samples, regardless of their geometric configuration. A total of 1,020 samples are used in this last section to test the performance of the tiered-filter approach.

5.2 Library of Explosive Templates

The library of explosive templates used in these results is composed of 126 artificial templates. All of them were developed for the same geometric configuration. This geometric configuration has been labeled in this study as the default configuration. Only 3 of the 126 templates are applied to the samples that have densities higher than 3 g/cm^3. These templates consist only of the filler elements (density values and filler elements listed on Table 5.2, with chemical composition #1 of Table 5.3). The other 123 templates are applied to the samples that have densities lower than 3 g/cm^3. This permits a crude application of the density tier described in Section 3.4.2.

The artificial clutter in front of the cyclonite explosive is, in the default configuration, 74 cm from the neutron source, the clutter is 10 cm thick, the distance between the clutter and the explosive is 1 cm, and the thickness of the explosive is 10 cm (total volume of 3,048 cm^3). The filler elements used, their corresponding densities, and the chemical composition of the clutter in front of the templates, are shown in tables 5.1, 5.2, 5.3, and 5.4.

Table 5.1. Density Values and Filler Elements for Templates in the Lower Density

Density	Value	Range	Filler element
Very Low Density	0.25	0 – 0.5	Li
Very Low Density	0.25	0 – 0.5	F
Low Density	1.0	0.5 – 1.5	Li
Low Density	1.0	0.5 – 1.5	F
Low Density	1.0	0.5 – 1.5	P
Medium Density	2.25	1.5 – 3.0	F

Table 5.2. Density Values and Filler Elements for Templates in the Higher Density Tier

Density	Value	Range	Filler Element
Medium Density	2.25	1.5 – 3.0	Cr
High Density	7.0	3.0 – 11.0	P
High Density	7.0	3.0 – 11.0	Cr

Table 5.3. Chemical Composition of Clutter Material with Filler Elements of Templates

	Nitrogen	Oxygen	Carbon	Hydrogen	Filler Element
1	0%	0%	0%	0%	100%
2	0%	0%	30%	60%	10%
3	0%	10%	30%	50%	10%
4	0%	20%	0%	0%	80%
5	0%	20%	20%	50%	10%
6	0%	30%	0%	30%	40%
7	0%	40%	0%	50%	10%
8	0%	40%	10%	0%	50%
9	0%	50%	0%	0%	50%
10	0%	60%	0%	0%	40%
11	0%	60%	20%	0%	20%
12	0%	70%	0%	0%	30%

Table 5.4. Chemical Composition of Clutter Material without Filler Elements of Templates

	Nitrogen	Oxygen	Carbon	Hydrogen
1	0%	0%	100%	0%
2	0%	0%	30%	70%
3	0%	0%	40%	60%
4	0%	0%	50%	50%
5	0%	10%	20%	70%
6	0%	10%	30%	60%
7	0%	20%	20%	60%
8	0%	20%	30%	50%
9	0%	20%	40%	40%
10	0%	30%	0%	70%
11	0%	80%	10%	10%
12	10%	0%	30%	60%
13	10%	0%	40%	50%
14	10%	10%	30%	50%
15	10%	10%	40%	40%
16	10%	10%	50%	30%
17	20%	0%	30%	50%

5.3 Materials Used for Explosive Clutter and Inert Samples

A wide range of materials was selected to test the tiered-filter approach. A total of 51 different materials, with densities ranging between 0.0012 g/cm^3 to 11.35 g/cm^3 were used as inert targets and as clutter in front of the explosives. These materials were employed in all the samples of the different geometrical configurations utilized to evaluate the performance of the tiered-filter approach. Because there are ten different geometric configurations, the total sum of inert and explosive targets equals 1020. Table 5.5 contains the list of materials used in this study.

Table 5.5. List of Materials Used as Clutter and as Inert Samples

1	Air	18	Gasoline	35	Polyurethane
2	Aluminum	19	Glass	36	Propane
3	Antifreeze	20	Granite	37	Rubber
4	Ash	21	Herbicide 1	38	Salt
5	Borax	22	Herbicide 2	39	Soap
6	Bricks	23	Herbicide 3	40	Soil
7	Carbon	24	K Hydroxide	41	Soy
8	Cardboard	25	Lead	42	Steel
9	Ceramic	26	Limestone	43	Styrofoam
10	Cherrywood	27	Lucite	44	Sugar
11	Concrete	28	Nickel	45	Tissue
12	Copper	29	Nylon	46	Titanium
13	Cotton	30	Petroleum	47	Void
14	Cyanurate	31	Plexiglass	48	Water
15	Ethanol	32	Polyethylene	49	Wax
16	Fertilizer A	33	Polypropylene	50	Woodoak
17	Fertilizer B	34	Polystyrene	51	Zirconium

5.4 Results for Samples with the Same Geometrical Configuration as Library Templates

The results shown in this section have the purpose of fixing all the variable factors that can affect the response of a target, and focus only on the chemical composition and density of the clutter. This was done to test how well the artificial materials used as clutter in the artificial explosive templates perform.

The geometrical configuration of the targets is the same as the one for the templates in the library. For the explosive samples, the clutter in front of the cyclonite explosive is 74 cm from the neutron source, the clutter is 10 cm thick, the distance between the clutter and the

explosive is 1 cm, and the thickness of the explosive is 10 cm. For the inert samples, the same configuration applies, keeping in mind that the volume occupied by the explosive is replaced with the same inert material as the clutter.

Table 5.6 and Table 5.7 show the number of True Positives, False Negatives, True Negatives, and False Positives, as well as the Sensitivity, Specificity, and objective function Omega obtained for this set of targets using the tiered-filter approach and the non-tiered approach, respectively. Each table consists of the results for the lower density tier, the higher density tier, as well as the final results. The cut-off values for each tier of the TFA and the cut-off value for the non-tiered approach, as well as the False Negatives and False Positives for both methods are given in Appendix D1.

Table 5.6. Results Using the Tiered Approach on Samples with the Same Geometrical Configuration as the Default Configuration

	Lower Density Tier	Higher Density Tier	Final Results
True Positives	44	5	49
False Negatives	1	1	2
True Negatives	42	6	48
False Positives	3	0	3
Sensitivity	0.978	0.833	0.961
Specificity	0.933	1	0.941
Ω	0.956	0.917	0.951

Table 5.7. Results Using the Non-Tiered Approach on Samples with the Same Geometrical Configuration as the Default Configuration

	Lower Density Tier	Higher Density Tier	Final Results
True Positives	44	6	50
False Negatives	1	0	1
True Negatives	40	6	46
False Positives	5	0	5
Sensitivity	0.978	1	0.980
Specificity	0.889	1	0.902
Ω	0.933	1	0.941

5.5 Results for Samples at Different Distances from the Source

In this section, the goal was to isolate and study the effect of moving the target to a position closer to the source. Two geometrical configurations different from the default configuration were simulated, one where the clutter and the explosive are both moved 10 cm closer to the source, and the other one where the clutter and the explosive are both moved 20 cm closer to the source. The purpose was to observe how well the artificial templates for a single separation perform for different separations in the tiered-filter approach.

Table 5.8 through Table 5.11 show the number of True Positives, False Negatives, True Negatives, False Positives, the Sensitivity, Specificity, and the objective function Omega implementing the tiered-filter approach and the non-tiered approach to the targets moved 10 cm and 20 cm closer to the source. The same parameters are shown in Table 5.12 and 5.13 for the combined results obtained by applying the library of templates to the targets moved 10 cm and 20 cm, as well as the default configuration targets, for a total of 182 samples. Each table consists of the results for the lower density tier, the higher density tier, as well as the final results. The

cut-off values for each tier of the TFA and the cut-off value for the non-tiered approach, as well as the samples labeled False Negatives and False Positives for both methods are given in Appendix D2.

Table 5.8. Results Using the Tiered Approach on Samples 10 cm Closer to the Source than the Default Configuration

	Lower Density Tier	Higher Density Tier	Final Results
True Positives	44	5	49
False Negatives	1	1	2
True Negatives	42	6	48
False Positives	3	0	3
Sensitivity	0.978	0.833	0.961
Specificity	0.933	1	0.941
Ω	0.956	0.917	0.951

Table 5.9. Results Using the Non-Tiered Approach on Samples 10 cm Closer to the Source than the Default Configuration

	Lower Density Tier	Higher Density Tier	Final Results
True Positives	44	6	50
False Negatives	1	0	1
True Negatives	35	6	41
False Positives	10	0	10
Sensitivity	0.978	1	0.980
Specificity	0.778	1	0.804
Ω	0.878	1	0.892

Table 5.10. Results Using the Tiered Approach on Samples 20 cm Closer to the Source than the Default Configuration

	Lower Density Tier	Higher Density Tier	Final Results
True Positives	43	6	49
False Negatives	2	0	2
True Negatives	42	6	48
False Positives	3	0	3
Sensitivity	0.956	1	0.961
Specificity	0.933	1	0.941
Ω	0.944	1	0.951

Table 5.11. Results Using the Non-Tiered Approach on Samples 20 cm Closer to the Source than the Default Configuration

	Lower Density Tier	Higher Density Tier	Final Results
True Positives	37	6	43
False Negatives	8	0	8
True Negatives	33	6	39
False Positives	12	0	12
Sensitivity	0.822	1	0.843
Specificity	0.733	1	0.765
Ω	0.789	1	0.804

Table 5.12. Results Using the Tiered Approach on Samples from the Default Configuration as well as Samples 10 cm and 20 cm Closer to the Source

	Lower Density Tier	Higher Density Tier	Final Results
True Positives	131	6	137
False Negatives	4	0	4
True Negatives	126	6	132
False Positives	9	0	9
Sensitivity	0.970	1	0.972
Specificity	0.933	1	0.936
Ω	0.952	1	0.954

Table 5.13. Results Using the Non-Tiered Approach on Samples from the Default Configuration as well as Samples 10 cm and 20 cm Closer to the Source

	Lower Density Tier	Higher Density Tier	Final Results
True Positives	111	18	117
False Negatives	24	0	24
True Negatives	114	18	120
False Positives	21	0	21
Sensitivity	0.822	1	0.830
Specificity	0.844	1	0.851
Ω	0.833	1	0.840

5.6 Results for Samples with Different Explosive Volume

The results presented in this section help isolate the effect caused by increasing the explosive volume. Three geometrical configurations different from the default configuration were simulated. The clutter position (74 cm from the neutron source), the clutter thickness (10 cm), and the distance between the clutter and the explosive (1 cm) are the same for these three

configurations as for the default one. The cross sectional area of the explosive remains the same for these configurations as the default one, but the explosive thicknesses are 15 cm (4572 cm^3), 20 cm (6096 cm^3), and 25 cm (7620 cm^3), respectively. The objective was to see if the artificial templates are flexible enough to identify explosive targets that possess explosive volumes larger than the ones for which the templates were originally designed.

Table 5.14 through Table 5.19 show the number of True Positives, False Negatives, True Negatives, False Positives, the Sensitivity, Specificity, and the objective function Omega employing the tiered-filter approach and the non-tiered approach to targets having explosive volumes of 4,572 cm^3, 6,096 cm^3, and 7,620 cm^3. The same parameters are shown in Table 5.20 and 5.21 for the combined results obtained by applying the library of templates to the previous mentioned targets in addition to the default configuration targets, for a total of 408 samples. Each table consists of the results for the lower density tier, the higher density tier, as well as the final results. Cut-off values for each tier of the TFA and the cut-off value for the non-tiered approach, False Negatives, and False Positives for both methods are given in Appendix D3.

Table 5.14. Results Using the Tiered Approach on Samples with Explosive 5 cm Thicker than the Default Configuration

	Lower Density Tier	Higher Density Tier	Final Results
True Positives	45	6	51
False Negatives	0	0	0
True Negatives	42	6	48
False Positives	3	0	3
Sensitivity	1	1	1
Specificity	0.933	1	0.941
Ω	0.967	1	0.971

Table 5.15. Results Using the Non-Tiered Approach on Samples with Explosive 5 cm Thicker than the Default Configuration

	Lower Density Tier	Higher Density Tier	Final Results
True Positives	44	6	50
False Negatives	1	0	1
True Negatives	35	5	40
False Positives	10	1	11
Sensitivity	0.978	1	0.980
Specificity	0.778	0.833	0.784
Ω	0.878	0.917	0.882

Table 5.16. Results Using the Tiered Approach on Samples with Explosive 10 cm Thicker than the Default Configuration

	Lower Density Tier	Higher Density Tier	Final Results
True Positives	45	4	49
False Negatives	0	2	2
True Negatives	41	6	47
False Positives	4	0	4
Sensitivity	1	0.667	0.961
Specificity	0.911	1	0.922
Ω	0.956	0.833	0.941

Table 5.17. Results Using the Non-Tiered Approach on Samples with Explosive 10 cm Thicker than the Default Configuration

	Lower Density Tier	Higher Density Tier	Final Results
True Positives	44	6	50
False Negatives	1	0	1
True Negatives	32	5	37
False Positives	13	1	14
Sensitivity	0.978	1	0.980
Specificity	0.711	0.833	0.725
Ω	0.844	0.917	0.853

Table 5.18. Results Using the Tiered Approach on Samples with Explosive 15 cm Thicker than the Default Configuration

	Lower Density Tier	Higher Density Tier	Final Results
True Positives	45	5	50
False Negatives	0	1	1
True Negatives	42	6	48
False Positives	3	0	3
Sensitivity	1	0.833	0.980
Specificity	0.933	1	0.941
Ω	0.967	0.917	0.961

Table 5.19. Results Using the Non-Tiered Approach on Samples with Explosive 15 cm Thicker than the Default Configuration

	Lower Density Tier	Higher Density Tier	Final Results
True Positives	32	6	38
False Negatives	13	0	13
True Negatives	33	6	39
False Positives	12	0	12
Sensitivity	0.711	1	0.745
Specificity	0.733	1	0.765
Ω	0.722	1	0.755

Table 5.20. Results Using the Tiered Approach on Samples from the Default Configuration as well as with Explosives 5, 10 and 15 cm Thicker

	Lower Density Tier	Higher Density Tier	Final Results
True Positives	179	18	197
False Negatives	1	6	7
True Negatives	168	24	192
False Positives	12	0	12
Sensitivity	0.994	0.750	0.966
Specificity	0.933	1	0.941
Ω	0.964	0.875	0.953

Table 5.21. Results Using the Non-Tiered Approach on Samples from the Default Configuration as well as with Explosives 5, 10 and 15 cm Thicker

	Lower Density Tier	Higher Density Tier	Final Results
True Positives	166	24	190
False Negatives	14	0	14
True Negatives	132	24	156
False Positives	48	0	48
Sensitivity	0.922	1	0.925
Specificity	0.733	1	0.742
Ω	0.828	1	0.833

5.7 Results for Samples with Different Clutter Thickness

In this section, the effect of clutter thickness was isolated by developing configurations with clutter thicknesses larger than the default case. Four geometrical configurations different from the default configuration were simulated. The thickness of the clutter in these configurations is increased from the front. Therefore, the explosive remains with the same volume (3,048 cm^3), in the same location, and at the same distance from the clutter (1 cm) as the default case, but the clutter increases in thickness and at the same time the front part of the clutter gets closer to the neutron source. The clutter thicknesses for these four configurations are 15 cm, 20 cm, 25 cm, and 30 cm. The goal is to study how well the artificial templates perform when applied to clutter thicknesses larger than they were designed and what their limitations are.

The number of True Positives, False Negatives, True Negatives, False Positives, the Sensitivity, Specificity, and the objective function Omega calculated using the tiered-filter approach and the non-tiered approach to this set of targets are shown in Tables 5.22 through Table 5.29. These parameters are also shown in Table 5.30 and 5.31 for the combined results

obtained by applying the library of templates to the previous mentioned targets in addition to the default configuration targets, for a total of 510 samples. Each table consists of the results for the lower density tier, the higher density tier, as well as the final results. The cut-off values for each tier of the tiered-filter approach and the cut-off value for the non-tiered approach, and the samples labeled False Negatives and False Positives for both methods are given in Appendix D4.

Table 5.22. Results Using the Tiered Approach on Samples with Clutter 5 cm Thicker than the Default Configuration

	Lower Density Tier	Higher Density Tier	Final Results
True Positives	45	6	51
False Negatives	0	0	0
True Negatives	40	6	46
False Positives	5	0	5
Sensitivity	1	1	1
Specificity	0.889	1	0.902
Ω	0.944	1	0.951

Table 5.23. Results Using the Non-Tiered Approach on Samples with Clutter 5 cm Thicker than the Default Configuration

	Lower Density Tier	Higher Density Tier	Final Results
True Positives	43	6	49
False Negatives	2	0	2
True Negatives	32	5	37
False Positives	13	1	14
Sensitivity	0.956	1	0.961
Specificity	0.711	0.833	0.725
Ω	0.833	0.917	0.843

Table 5.24. Results Using the Tiered Approach on Samples with Clutter 10 cm Thicker than the Default Configuration

	Lower Density Tier	Higher Density Tier	Final Results
True Positives	43	6	49
False Negatives	2	0	2
True Negatives	40	6	46
False Positives	5	0	5
Sensitivity	0.956	1	0.961
Specificity	0.889	1	0.902
Ω	0.922	1	0.931

Table 5.25. Results Using the Non-Tiered Approach on Samples with Clutter 10 cm Thicker than the Default Configuration

	Lower Density Tier	Higher Density Tier	Final Results
True Positives	27	6	33
False Negatives	18	0	18
True Negatives	42	5	47
False Positives	3	1	4
Sensitivity	0.600	1	0.647
Specificity	0.933	0.833	0.922
Ω	0.767	0.917	0.784

Table 5.26. Results Using the Tiered Approach on Samples with Clutter 15 cm Thicker than the Default Configuration

	Lower Density Tier	Higher Density Tier	Final Results
True Positives	45	6	51
False Negatives	0	0	0
True Negatives	39	6	45
False Positives	6	0	6
Sensitivity	1	1	1
Specificity	0.867	1	0.882
Ω	0.933	1	0.941

Table 5.27. Results Using the Non-Tiered Approach on Samples with Clutter 15 cm Thicker than the Default Configuration

	Lower Density Tier	Higher Density Tier	Final Results
True Positives	26	6	32
False Negatives	19	0	19
True Negatives	38	5	43
False Positives	7	1	8
Sensitivity	0.578	1	0.627
Specificity	0.844	0.833	0.843
Ω	0.711	0.917	0.735

Table 5.28. Results Using the Tiered Approach on Samples with Clutter 20 cm Thicker than the Default Configuration

	Lower Density Tier	Higher Density Tier	Final Results
True Positives	38	6	44
False Negatives	7	0	7
True Negatives	40	5	45
False Positives	5	1	6
Sensitivity	0.844	1	0.863
Specificity	0.889	0.833	0.882
Ω	0.867	0.917	0.873

Table 5.29. Results Using the Non-Tiered Approach on Samples with Clutter 20 cm Thicker than the Default Configuration

	Lower Density Tier	Higher Density Tier	Final Results
True Positives	23	6	29
False Negatives	22	0	22
True Negatives	40	5	45
False Positives	5	1	6
Sensitivity	0.511	1	0.569
Specificity	0.889	0.833	0.882
Ω	0.700	0.917	0.725

Table 5.30. Results Using the Tiered Approach on Samples from the Default Configuration as well as with Clutter 5, 10, 15 and 20 cm Thicker

	Lower Density Tier	Higher Density Tier	Final Results
True Positives	217	28	245
False Negatives	8	2	10
True Negatives	200	30	230
False Positives	25	0	25
Sensitivity	0.964	0.933	0.961
Specificity	0.889	1	0.902
Ω	0.927	0.967	0.931

Table 5.31. Results Using the Non-Tiered Approach on Samples from the Default Configuration as well as with Clutter 5, 10, 15 and 20 cm Thicker

	Lower Density Tier	Higher Density Tier	Final Results
True Positives	176	30	206
False Negatives	49	0	49
True Negatives	174	25	199
False Positives	51	5	56
Sensitivity	0.782	1	0.808
Specificity	0.773	0.833	0.780
Ω	0.778	0.917	0.794

5.8 Results for All Samples Combined

In this section, the library of templates is applied to all the target samples, regardless of their geometric configuration. A total of 1,020 samples are used in this last section to test the performance of the tiered-filter approach. The results for the non-tiered approach are also presented for comparison.

The number of True Positives, False Negatives, True Negatives, False Positives, the Sensitivity, Specificity, and the objective function Omega calculated using the tiered-filter approach and the non-tiered approach to this set of targets are shown in Tables 5.32 and Table 5.33. Each table consists of the results for the lower density tier, the higher density tier, as well as the final results. The cut-off values for each tier of the tiered-filter approach and the cut-off value for the non-tiered approach, and the samples labeled False Negatives and False Positives for both methods are given in Appendix D5.

Table 5.32. Results Using the Tiered Approach On

All Samples Generated for this Study

	Lower Density Tier	Higher Density Tier	Final Results
True Positives	442	49	491
False Negatives	8	11	19
True Negatives	399	60	459
False Positives	51	0	51
Sensitivity	0.982	0.817	0.963
Specificity	0.887	1	0.900
Ω	0.934	0.908	0.931

Table 5.33. Results Using the Non-Tiered Approach On All Samples Generated for this Study

	Lower Density Tier	Higher Density Tier	Final Results
True Positives	388	55	443
False Negatives	62	5	67
True Negatives	324	58	382
False Positives	126	2	128
Sensitivity	0.862	0.917	0.869
Specificity	0.720	0.967	0.749
Ω	0.791	0.942	0.809

CHAPTER 6 – SUMMARY, CONCLUSIONS, AND RECOMMENDATIONS

6.1 Summary

This study addresses the problem of distinguishing unknown targets that contain nitrogen-rich explosive samples from ones that contain non-explosive materials only. The method proposed to solve this problem is called the tiered-filter approach, and is based on the signature-based radiation scanning technique [2]. The approach consists on calculating a normalized figure-of-merit between signatures from an unknown target and signatures from an explosive template through tiers (nitrogen first, then oxygen, then carbon, and finally hydrogen). If the normalized figure-of-merit is greater than a specified cut-off value for any given tier, then that specific template would not match the target and the process would be repeated for the next explosive template until all of the applicable templates have been evaluated. If the signatures of the unknown target match all the tiers of a particular template, then the target is assumed to contain an explosive.

An important component of the method is to develop a systematic methodology for constructing a library of templates that identifies explosives under different target configurations. This was achieved by developing artificial explosive templates. Artificial explosive templates are constructed from signatures for a target that contains a real explosive with an artificial inert material used as clutter. These artificial materials have the function of representing all the different real inert materials that can occur in the field. Additionally, artificial explosive templates are constructed or different values of other variables, such as explosive size.

A function called Omega was developed in section 3.5.2 to evaluate the performance of the technique. This function takes into account the sensitivity and specificity of the method. It also serves to optimize parameters in the tiered-filter approach. The simulated annealing

algorithm based on the downhill simplex method was used together with the Omega function to optimize the results for the different cases evaluated.

Computer simulations using MCNP were performed instead of real experiments. The simulation geometry, the explosive and inert samples, as well as a detailed description of how the artificial explosive templates were constructed were described in Chapter 4. The optimized results from the simulated data for all the different cases studied are presented in Chapter 5.

6.2 Conclusions

This section discusses in detail the results shown in Chapter 5, and draws conclusions from them. The study concentrated on the following four main variables that affect the performance of the artificial explosive templates:

- Chemical composition and density of artificial clutter materials
- Distance of the target from the neutron source
- Explosive volume
- Clutter thickness.

Results in Chapter 5 were obtained by using the tiered-filter approach and the non-tiered approach. Even though the original non-tiered approach makes use of no tier at all, in this study the density tier was applied to both methods. This makes a proper evaluation of the HCNO tiers possible by making every other parameter equal. The sensitivities and specificities shown in the tables of Chapter 5 describe how well the methods perform. The Omega function gives equal weight to both the sensitivity and the specificity to give a single value that enables the comparison between both methods. The reasons why some samples resulted in False Positives or False Negatives are also discussed and analyzed.

6.2.1 Samples with Same Geometric Configuration as Library of Templates

The results in section 5.4 and Appendix D1 focus on the chemical composition and density of the clutter material. The goal was to test if artificially specified materials and use of discrete values of density can be used effectively to represent clutter in the explosive templates. All the other variables were fixed.

Table 5.6 and Table 5.7 show that the artificial templates give results for Sensitivity, Specificity, and Omega, above 90%. The sensitivity of the non-tiered approach was slightly better than that for the tiered approach. This was because the tiered approach had 1 False Negative (Titanium) from the Higher Density tier samples, while the non-tiered approach had none. On the other hand, the specificity was slightly better for the tiered approach. In particular, this is one situation to be expected because the tiered-filter approach makes it significantly more difficult for non-explosive samples lacking enough nitrogen to be confused with nitrogen-rich explosives. This is illustrated by the fact that the targets containing tissue and water led to two False Positives (which contained no or very little Nitrogen). The Omega objective function, which gives in this study equal weight to the sensitivity and the specificity, indicates that the tiered approach is slightly better than the non-tiered one.

6.2.2 Samples at Different Distances from the Source

The objective of the results shown in section 5.5 and Appendix D2 was to isolate the effect of changing the position of the samples and to evaluate how well the artificial templates designed for a particular distance would perform at evaluating samples at different distances. In this study, the samples were moved closer to the source compared to the sample locations for the library of templates.

Tables 5.8, 5.9, 5.10, 5.11 indicate that the tiered-filter approach gave results for the

sensitivity, specificity, and Omega that were all above 94%, while the non-tiered approach gave results that were between 80% and 90%. The False Positives, False Negatives, and cut off values for N and O, are very similar for all tiered-filter approach cases, including the default shown in Table 5.6. The False Positives and False Negatives from the non-tiered approach, shown in Tables 5.9 and 5.11, increased significantly compared to the default configuration presented in Table 5.7. In particular, the specificity decreased appreciably. The results seem to indicate that the non-tiered approach is considerably more sensitive to changes in distance of the target than are the tiered results. Several materials that don't contain N were confused as explosives in the non-tiered approach. From these observations, it can be concluded that the tiered-filter approach is less sensitive to the specific location of the sample in the target than is the non-tiered approach.

The results from Table 5.12 seem to show further proof that slightly different changes in distance don't affect the sensitivity and specificity of a library of templates when the tiered-filter method is used. On the other hand, Table 5.13 indicates that significantly more False Negatives arise when samples at different distances from the source are evaluated. In this particular study, the difference in optimal cut-off values for different configurations is responsible for explaining the drastic increase in False Negatives. The default and 10 cm closer to the target configuration had a cut-off value of 4, while the 20 cm closer configuration had a cut-off value of 6. The optimal cut-off value calculated from combining these three configurations turned out to be 4, which severely increased the number of False Negatives from the 20 cm closer configuration.

In the simulations performed in this study, the beam was perfectly collimated. Under those circumstances, the tiered-filter approach gave very excellent results. This study practically indicates that reasonable changes in position of the target (closer or further from the neutron

source) should not represent a major obstacle for a particular artificial explosive template to perform well. This is important because if beams are well collimated in actual tests then this study indicates that the tiered filter approach requires significantly fewer templates for different distances from the source.

6.2.3. Samples with Different Explosive Volumes

The purpose of the results shown in section 5.6 and Appendix D3 was to study how flexible the artificial templates are in terms of evaluating targets with different explosive volumes. It should be noted that the volume of the corresponding inert samples increased as well.

Tables 5.14, 5.15, 5.16, 5.17, 5.18, and 5.19 give sensitivity, specificity, and Omega results above 94% for the tiered-filter approach, and results above 72% for the non-tiered approach. For the Lower Density Tier, the sensitivity of the tiered-filter approach was 100% for all these cases, while the specificity was lower, but still above 91%. For the Higher density tier, the results were reversed, given that the specificity was 100% while the sensitivity decreased significantly. The results for the lower tier occurred because larger explosive volumes contain significantly more N, which non-explosive samples don't have. Therefore, fewer False Negatives result at the end of the nitrogen tier. However, non-explosive nitrogen rich samples would also have their volume increased, making the nitrogen tier less effective against them, thus increasing the number of False Positives. Fertilizer, Herbicide 1, and Nylon appear as False Positives on all cases because they contain significant amount of nitrogen, and a relatively similar chemical composition to explosives.

In the case of the Higher Density Tier for the tiered approach, the inert materials (pure metals with very high density) do not contain any nitrogen. Hence, very few False Positives result. On the other hand, because several nitrogen net peaks are significantly smaller for higher

tiers, then recognizing a sample as an explosive relies more on the other signatures (hydrogen, carbon, and oxygen). This makes explosives harder to identify, thus yielding a higher number of False Negatives. In spite of these shortcomings, the Omega functions for the tables showing the results for the tiered approach are all above 94%.

The results for the non-tiered approach were not as promising as the tiered filter ones. The Omega functions ranged from 75% to 88%. The sensitivity and the specificity for the Higher Density Tier were relatively high, but the specificity for the Lower Density Tier brought the overall performance down. The sensitivities for the 5 cm and 10 cm thicker cases were 97.8% for both, but for the 15 cm case it was only 71.1%. The fact that the specificity is considerably affected points to the advantage that the tiered approach has over the non-tiered one, where the nitrogen tier significantly reduces False Positives.

Table 5.20 shows that the two main sources that reduce the Omega function are the Lower Density Tier Specificity and the Higher Density Tier Sensitivity. The 12 False Positives that reduced the Lower Density Sensitivity Tier were the Fertilizer, Herbicide 1, and Nylon cluttered samples from the four different geometric configurations. All of them contain significant amounts of N and, as stated before, concentrations of Hydrogen, Carbon, and Oxygen that makes it difficult to distinguish them from explosive samples. The main contributors to decreasing the Higher Density Tier Sensitivity was the Titanium inert sample and, at a smaller scale, the Zirconium inert sample. Table 5.21 shows that the main weakness of the non-tiered approach for dealing with samples with larger explosive (and inert) volume are the large amount of False Positives, which turned out to be four times as much as the tiered approach.

6.2.4 Samples with Different Clutter Thickness

The objective of the results shown in section 5.7 and Appendix D4 was to isolate the effect of the clutter thickness, and study how well the artificial templates designed for a specific clutter thickness perform at evaluating a sample with a clutter having a different thickness. The thickness of the clutter was increased from the front for the samples generated in this study.

Tables 5.22, 5.24, 5.26, and 5.28, show the results for the tiered-filter approach. The sensitivity, specificity, and the Omega functions for these configurations yielded results above 88%. In general, the number of False Negatives for all these cases was very low, which resulted in very high sensitivities, above 95%. The only exception was the case with the thickest clutter, which gave a Lower Density Tier sensitivity of 84%, and an overall sensitivity of 86%. Clearly the weakest performance of the tiered-filter approach for samples with different clutter was the Lower Density Tier specificity. The results were between 86 and 89%. However, the Omega function values which reflect the overall performance of the method 87% and 95%. From Appendix D4 that most of the False Positives from the different configurations are the Fertilizer A, Herbicide 1, Nylon, Polyurethane, and Tissue inert samples. All of these inert samples contain some amount of nitrogen, which added to the large volumes of clutter increases the difficulty for the nitrogen tier to filter samples more effectively.

The results for the non-tiered approach are shown in Tables 5.23, 5.25, 5.27, and 5.29. The values for the sensitivity, specificity, and the Omega functions for these configurations range between 56% and 96%. In general, the Lower Density Tier sensitivity yields the weaker performance, except for the results from the 15 cm thick clutter (in this configuration the specificity is significantly smaller). The Omega function values range between 72% and 84%. Comparing these performance values with the tiered-filter approach values, indicates a clear

advantage in the use of tiers to better handle the clutter thickness problem.

Table 5.30 indicates that samples with thicker clutter will increase the number of False Positives particularly for the Lower Density Tier. The clutter thickness problem is clearly the most difficult for the tiered-filter approach to overcome, which means more templates of different thicknesses would be required to improve the results. In spite of this, the Omega values for clutter up to 15 cm thicker than the artificial templates were above 93%, which can be considered promising. The results of Table 5.31 indicate that most False Positives and False Negatives came from the Lower Density Tier. This again illustrates the significant advantage that filtering targets through a nitrogen tier, in particular, offers.

6.2.5 All Samples Combined

Finally, all the explosive and inert samples generated in this study were evaluated and the results are shown in Table 5.32, Table 5.33, and Appendix D5. A total of 1020 samples were used to test the performance of the tiered filter approach. As can be seen in Table 5.3.2 the Higher Density Tier sensitivity and the Lower Density Tier specificity, were the areas that decreased the overall performance of the tiered-filter method. The Lower Density Tier specificity was reduced by the inert samples such as Fertilizer A, Herbicide 1, and Nylon, that because of their N content and chemical composition similar enough to explosives, proved to be the main weakness of the method. Nevertheless, by identifying this "problem" samples, additional tiers can be employed that can identify characteristic signatures of these inert materials and be able to filter them. The Higher Density Tier sensitivity was affected mainly by the titanium and, to a lesser degree, by the zirconium cluttered explosive samples. The problem might be arising from the lower nitrogen net peaks from these metals. In here the problem might be solved by developing artificial clutter materials that are closer to that of the formerly mentioned metals. It should also

be noticed that the non-tiered approach shown in Table 5.33 gave better results for the Higher Density Tier samples. Therefore, it could be better to use the non-tiered approach to evaluate samples when the Higher Density Tier is used.

6.3 Recommendations for Future Research

Two possible avenues exist to develop the library of templates necessary for the tiered-filter approach to be successfully applied in the field. One way is to develop this library experimentally using real materials that can take the role of the artificial materials described in this study. If materials that have the flexibility required to represent all other real materials exist or can be generated needs to be figured out. The other avenue is to make the MCNP simulations as accurate and realistic as possible. This can be done by comparing and constantly improving the net peaks of the different signatures from the simulations with the ones obtained from real experimental samples. Simulations should take into account all the inefficiencies the detectors and other components can have. Elements other than Li, F, P, and Cr can be tried to see if the results improve. The discrete values of the relevant parameters in the artificial templates (such as density, clutter thickness, target position, explosive thickness, etc.) can be made finer or more coarse, depending on how well they react to changes and how well they compare to real experimental samples.

One aspect that was not developed in the present study, but that could prove to be very useful in the field when applying the tiered-filter approach, is to offer a third option of identifying the target as a suspect. This means that if the system cannot be certain enough about a target being an explosive or not, it can indicate it to the user, so that other methods of bomb detection can be used.

Whenever the tiered filter approach cannot identify with enough certainty (predetermined by the

user) that a target is an explosive, the option of labeling the target as a suspect can be offered. The traditional definitions of sensitivity and specificity do not include samples labeled as suspects. Therefore, the sensitivity and specificity of the system can be redefined. The aim of the new definition of these terms is to do it in such a way that the inclusion of suspect samples is a natural extension of the traditional definition of the terms. Table 6.1 shows the possible combinations that can occur if the detection system is allowed to label some targets as suspects. In Table 6.1 S_E stands for explosives labeled as suspects and S_I stands for non-explosive (inert) samples labeled as suspects.

Table 6.1 Detector Output vs True Status of Test for IED Detection Systems Including Targets Labeled as Suspects

	Explosive Was Present	No Explosive Was Present
Detector Indicated Explosive was Present	True Positive (L_E)	False Positive (M_I)
Detector Labeled Target as Suspect	True Suspect (S_E)	False Suspect (S_I)
Detector Indicated No Explosive was Present	False Negative (M_E)	True Negative (L_I)
	Total Number of Explosive Targets (N_E)	Total Number of Non-Explosive Targets (N_I)

The original definition of sensitivity is based on the number of explosives that were correctly identified, divided by the total number of explosives. Therefore, the natural extension of the definition to include suspect samples would be to add the number of explosives and

explosive suspects that were correctly identified (True Positives and True Suspects), and divide them by the total number of explosives. However, a weight factor (smaller than unity) that penalizes the performance of the detection system should be given to the number of samples labeled as suspects, because the system was not able to label them as explosives with enough certainty. The definition of sensitivity developed in this study is given by

$$\varepsilon_n = \frac{L_E + \omega_S S_E}{N_E}, \qquad \omega_S < 1 \ , \tag{6.1}$$

where ε_n is the newly defined sensitivity factor, and ω_S is the suspect weight factor.

A similar analysis can be given to the definition of specificity. The original definition is based on the number of inert samples that were correctly identified, divided by the total number of inert samples. Now, inert samples labeled as suspects should be grouped with inert samples labeled as explosives, because the former has to undergo secondary tests to verify if it is an explosive or not. So, in this case the natural extension of the definition to include suspect samples requires that the original definition of specificity is written in terms of False Positives (inerts labeled as explosives) and False Suspects (inerts labeled as suspects). The suspect weight factor is also included and, contrary to the sensitivity, this factor improves the performance because False Suspects reduce the specificity by a lesser amount of than False Positives do. The definition of specificity developed in this study is given by

$$\varepsilon_p = \frac{L_I}{N_I} = \frac{N_I - (M_I + \omega_S S_I)}{N_I} \ . \tag{6.2}$$

REFERENCES

[1] Buffler, A. “Contraband Detection Using Fast Neutrons”, *Radiation Physics and Chemistry*, Department of Physics, University of Cape Town, Vol. 71, pp. 853-861, 2004.

[2] Dunn, W.L., Banerjee, A. Allen, J. Van Meter, “Feasibility of a method to identify targets that are likely to contain conventional explosives”, *Nuclear Instruments and Methods in Physics Research B*, Vol. 263, pp. 179-182, 2007.

[3] Loschke, K.W., W.L. Dunn, “Detection of chemical explosives using multiple photon signatures”, *Applied Radiation and Isotopes*, Vol. 68, pp. 884-887, 2010.

[4] Lowrey, J.D., W.L. Dunn, “Signature based radiation scanning using radiation interrogation to detect explosives”, *Applied Radiation and Isotopes*, Vol. 68, pp. 893-895, 2010.

[5] Guzman, R. (2007) ARNEWS. Joint IED Task Force helping Defuse Insurgency’s Threat. Retrieved July 7, 2008. <http://www.globalsecurity.org/military/intro/ied.htm>

[6] National Research Council, Existing and Potential Standoff Explosives Detection Techniques, National Academy PressWashington D.C. 2004.

[7] State Archival Service. "Historical background". *World War Two*. Republic of Belarus, Ministry of Justice, Department of Archives and Records Management. <http://www.archives.gov.by/eng/index.php?id=104476>.

[8], “Mine warfare in Vietnam”, *Human Rights Watch*, retrieved May 2012, from <http://www.hrw.org/reports/1997/gen1/General-03.htm. Retrieved 2009-10-18.>

[9] Smith, Steve, 3-2-1 Bomb Gone : Fighting Terrorist Bombers in Northern Ireland Sutton Publishing, pp. 131-149, 2006.

[10] "Operation Enduring Freedom", (2010-05-28), *iCasualties.org*, retrieved May 2012, from <http://icasualties.org/oef/>.

[11] "More Attacks, Mounting Casualties", (2007-09-30), *The Washington Post*, retrieved May 2012, from
<http://www.washingtonpost.com/wp-dyn/content/graphic/2007/09/28/GR2007092802161.html>.

[12] "Middle East | Iran 'behind attacks on British'", (2005-10-05), *BBC News*, retrieved May 2012, from <http://news.bbc.co.uk/2/hi/middle_east/4312516.stm.>

[13] "Middle East | Blair warns Iran over Iraq bombs", (2005-10-06), *BBC News*, retrieved May 2012, from <http://news.bbc.co.uk/2/hi/middle_east/4315924.stm>

[14] Shatz, A., "In Search of Hezbollah", (2004-03-31), *The New York Review of Books*, retrieved May 2012, from <http://www.nybooks.com/articles/archives/2004/apr/29/in-search-of-hezbollah/#fn1-763330970>.

[15] Grazioso, A., "The guerrilla warfare in Checnya and Iraq: A preliminary comparison", CASD CeMiSS Quarterly Summer 2005, CASD, pp. 31-40, 2005.

[16] "Mumbai Blasts: Death Toll rises to 26", (2011-07-30), *Hindustan Times*, retrieved May 2012, <http://www.hindustantimes.com/India-news/Mumbai/Mumbai-blasts-Death-toll-rises-to-26/Article1-727292.aspx>

[17] Michaels, J., "Use of IEDs by regime opposition in Syria rises sharply", (2012-03-04) *USA TODAY*, retrieved May 2012, from <http://usatoday30.usatoday.com/news/world/story/2012-03-04/syria-ieds/53357110/1>.

[18] Runkle, R.C., T.A. White, E.A. Miller, J.A. Caggiano, B.A. Collins, "Photon and neutron interrogation techniques for chemical explosives detection in air cargo: A critical review", *Nuclear Instruments and Methods in Physics Research A*, Vol. 603, pp. 510-528, 2009.

[19] Habiger, K.W., J.R. Clifford, R.B. Miller, W.F. McCullough, "EXDEP/CTX: An explosive detection system for screening luggage with high energy X-rays", *Proc. IEEE Particle Accelerator Conf.* 4, 2622-2624, 1994.

[20] Yinon, J. Forensic and Environmental Detection of Explosives; John Wiley & Sons: Chichester, UK, 1999.

[21] Jimenez, A.M., M.J. Navas, Detection of Explosives by Chemiluminescence in Counterterrorist Detection Techniques of Explosives, J.Yinon, Elsevier, Netherlands, pp. 139, 2007.

[22] Jimenez, A.M., M.J. Navas, "Chemiluminescence Detection Systems for the Analysis of Explosives", *Journal of Hazardous Materials*, Vol. 106A, pp. 1-8, 2004.

[23] Yinon, J., Detection of Explosives by Mass Spectrometry in Counterterrorist Detection Techniques of Explosives, J.Yinon, Elsevier, Netherlands, pp. 41-59, 2007.

[24] Steinfeld, J.I., J. Wormhoudt, "Explosives Detection: A Challenge for Physical Chemistry", *Annual Review Physics and Chemistry*, Vol. 49, pp. 203-32, 1998.

[25] Senesac, L., T. Thundat, Explosive Vapor Detection Using Microcantilever Sensors in Counterterrorist Detection Tehcniques of Explosives, J. Yinon, Elsevier, Netherlands, pp.109-130, 2007.

[26] Van Neste, C.W., L.R. Senesac, D. Yi, T. Thundat, "Standoff Detection of Explosive Residues Using Photothermal Microcantilevers", *Applied Physics Letters*, Vol. 92, 134102, 2008.

[27] Harper, R.J., K.G. furton, Biological Detection of Explosives in Counterterrorist Detection Techniques of Explosives, J. Yinon, Elsevier, Netherlands, pp. 395-431, 2007.

[28] Correa, J.E., "The Dog's Sense of Smell", Food and Animal Sciences, Alabama A&M University, July 2005. <http://www.aces.edu/pubs/docs/U/UNP-0066/>

[29] Singh, S., M. Singh, "Explosives Detection systems (EDS) for Aviation Security", *Signal Processing*, Vol. 83, pp. 31-55, 2003.

[30] Harding, G., "X-ray Scatter Tomography for Explosives Detection", *Radiation Physics and Chemistry*, Vol. 71, Elsevier, pp. 869-881, 2004.

[31] Kusnetzov, A., A. Evsenin, MS-SRIP – Microwave System for Secret Standoff Inspection of People in Stand-off Detection of Suicide Bombers and Mobile Suspects, H.Schubert and A. Rimski-Korsakov, Springer, pp. 5-10, 2006.

[32] Sheen, D.M., D.L. McMakin, T.E. Hall, Detection of Explosives by Millimeter-wave Imaging in Counterterrorist detection Techniques of Explosives, J. Yinon, elsevier, Netherlands, pp. 237-277, 2007.

[33] Garroway, A.N., M.L. Buess, J.B. Miller, B.H. Suits, A.D. Hibbs, G.A. Barall, R. Matthews, L.J. Burnett, "Remote Sensing by Nuclear Quadrupole Resonance", *IEEE Transactions on Geoscience and Remote Sensing*, Vol 39, No. 6, 2001.

[34] Rudakov, T.N., T.J.Rayner, P.A. Hayes, K.L. Russeth, Detection of Explosives by Quadrupole Resonance Method: New Aspects for Security in Detection and Disposal of Improvised Explosives, H. Schubert and A.Kuznetsov, Springer, Netherlands, pp. 191-204, 2006.

[35] Hussein, E.M., E.J. Waller, "Review of one-side approaches to radiographic imaging for detection of explosives and narcotics", *Radiation Measurements*, Vol.29, No. 6, pp. 581-591, 1998.

[36] Lanza, R.C., Neutron Techniques for Detection of Explosives in Counterterrorist Detection Technique of Explosives, J. Yinon, elsevier, Netherlands, pp. 131-155, 2007.

[37] Vourvopulos, G., P.C. Womble, "Pulsed fast/thermal neutron analysis: a technique for explosives detection", *Talanta*, Vol. 54, pp.459-468, 2001.

[38] Nelder, John A., R. Mead, "A simplex method for function minimization". *Computer Journal* 7, pp. 308–313, 1965.

[39] Hoffman, A. J., P. Wolfe, "History", in Lawler, Lenstra, Rinooy Kan and Shmoys, eds., The Traveling Salesman Problem: A Guided Tour of Combinatorial Optimization Wiley, pp. 1-16, 1985.

APPENDICES

APPENDIX A

In this Appendix a proof that the covariance terms between the variables U_j, K_{tj}, $\sigma^2(U_j)$, and $\sigma^2(K_{tj})$, equal identically zero (see section 3.3.2) is presented. First, it will be shown that the covariance between two variables that are independent equals identically zero. Then, it will be shown that the covariance between a variable and its variance also equals identically zero.

The covariance between any two real-valued random variables x and y with finite second moment is defined as

$$\operatorname{cov}(x, y) = E[(x - E[x])(y - E[y])] \tag{A.1}$$

where $E[x]$ and $E[y]$ are the expected values of x and y respectively. If x and y are independent variables, then their covariance is given by

$$\operatorname{cov}(x, y) = E[xy - xE[y] - yE[x] + E[x]E[y]]$$

Using the linear property of the expected value operator

$$= E[xy] - E[xE[y]] - E[yE[x]] + E[E[x]E[y]]$$

Factoring out the expected values inside the expected value operator, and using the fact that under independence $E[xy]=E[x]E[y]$ gives

$$= E[x]E[y] - E[y]E[x] - E[x]E[y] + E[x]E[y]E[1]$$

$$\equiv 0$$

Therefore, the covariance terms between U_j and K_{tj}, U_j and $\sigma^2(K_{tj})$, K_{tj} and $\sigma^2(U_j)$, and $\sigma^2(U_j)$ and $\sigma^2(K_{tj})$, equal zero.

Now it will be shown that the covariance between a variable and its variance equals identically zero. Starting with the definition of covariance

$$\operatorname{cov}(x,\sigma^2(x)) = E[(x - E[x])(\sigma^2(x) - E[\sigma^2(x)])] \tag{A.2}$$

Distributing the inside terms

$$= E[x\sigma^2(x) - xE[\sigma^2(x)] - E[x]\sigma^2(x) + E[x]E[\sigma^2(x)]]$$

Applying the expected value operator

$$= E[x\sigma^2(x)] - E[xE[\sigma^2(x)]] - E[E[x]\sigma^2(x)] + E[E[x]E[\sigma^2(x)]]$$

Because the expected values are constant, the expected values within others can be factored out. Doing so results in

$$= E[x\sigma^2(x)] - E[\sigma^2(x)]E[x] - E[x]E[\sigma^2(x)] + E[x]E[\sigma^2(x)]E[1]$$

Using the fact that the expected value of one is one, the last two terms cancel each other. The result is then

$$= E[x\sigma^2(x)] - E[\sigma^2(x)]E[x]$$

The definition of the variance a variable x is $\sigma^2(x)=E[x^2]-(E[x])^2$. Substituting this definition in the previous equation gives

$$= E[x\{E[x^2]-(E[x])^2\}]-E[\{E[x^2]-(E[x])^2\}]E[x]$$

Distributing the inside terms

$$= E[xE[x^2]-x(E[x])^2]-E[\{E[x^2]-(E[x])^2\}]E[x]$$

Factoring out the expected values within the expected value operators and simplifying

$$= E[x^2]E[x]-(E[x])^2E[x]-E[x^2]E[x]+(E[x])^2E[x]$$

$$\equiv 0$$

Therefore, it has been shown that the covariance between U_j and $\sigma^2(U_j)$, and K_{tj} and $\sigma^2(K_{tj})$ equal identically zero. Result which was used in section 3.3.2

APPENDIX B

In this Appendix the two approximations for the standard deviation of the figure-of-merit described in section 3.3.2 are derived. The figure-of-merit for the template-matching procedure developed by Dunn [3] is of the following chi-square-like form

$$\zeta_t = \sum_{j=1}^{J} \alpha_j \frac{\left(\beta U_j - K_{tj}\right)^2}{\beta^2 \sigma^2\left(U_j\right) + \sigma^2\left(K_{tj}\right)} \quad , \tag{B.1}$$

where U_j is the jth measured signature of an unknown sample, K_{tj} is the jth signature for the tth template, J is the number of signatures, β is a factor that scales the measured values to the template values, σ^2 is the variance, and α_j is a normalized weight factor defined as

$$\alpha_j = \frac{\omega_j}{\sum_{j=1}^{J} \omega_j}, \tag{B.2}$$

with ω_j being a positive weight for the jth signature. From Equation (B.2) it can be concluded that

$$\sum_{j=1}^{J} \alpha_j = 1, \tag{B.3}$$

An estimate of the standard deviation of this figure-of-merit has been derived from the propagation of errors formula [3]. The propagation of errors formula is given by

$$\sigma(f) = \left|\frac{\partial f}{\partial a}\right|^2 \sigma^2(a) + \left|\frac{\partial f}{\partial b}\right|^2 \sigma^2(b) + 2\frac{\partial f}{\partial a}\frac{\partial f}{\partial b}\operatorname{cov}(ab), \tag{B.4}$$

where f is any given function of the variables a and b, $\sigma^2(a)$ and $\sigma^2(b)$ are the variances of the variables a and b, respectively, and $cov(ab)$ is the covariance between these variables.

It was shown in Appendix A, that the covariance between two independent variables or the covariance between a variable and its variance equals identically zero. Therefore, the covariance terms between the variables U_j, K_{tj}, $\sigma^2(U_j)$, and $\sigma^2(K_{tj})$ equal zero. Subsequently, the standard deviation of the figure-of-merit of Eq. (B.1) simplifies to

$$\sigma(\zeta_t)=\left\{\sum_{j=1}^{J}\left[\frac{\partial\zeta_t}{\partial U_j}\right]^2\sigma^2(U_j)+\sum_{j=1}^{J}\left[\frac{\partial\zeta_t}{\partial K_{tj}}\right]^2\sigma^2(K_{tj})\right.$$
$$\left.+\sum_{j=1}^{J}\left[\frac{\partial\zeta_t}{\partial\sigma^2(U_j)}\right]^2\sigma^2\left(\sigma^2(U_j)\right)+\sum_{j=1}^{J}\left[\frac{\partial\zeta_t}{\partial\sigma^2(K_{tj})}\right]^2\sigma^2\left(\sigma^2(K_{tj})\right)\right\}^{1/2}. \tag{B.5}$$

The terms $\sigma^2(\sigma^2(U_j))$ and $\sigma^2(\sigma^2(K_{tj}))$ are known as the variance of the variance (VOV). The partial derivatives of each of the terms in Eq. (B.5) are

$$\frac{\partial\zeta}{\partial U_j}=\frac{2\alpha_j\beta(\beta U_j-K_{tj})}{\beta^2\sigma^2(U_j)+\sigma^2(K_{tj})}, \tag{B.6}$$

$$\frac{\partial\zeta}{\partial K_{tj}}=\frac{-2\alpha_j(\beta U_j-K_{tj})}{\beta^2\sigma^2(U_j)+\sigma^2(K_{tj})}, \tag{B.7}$$

$$\frac{\partial\zeta}{\partial\sigma^2(U_j)}=\frac{-\alpha_j\beta^2(\beta U_j-K_{tj})^2}{\left[\beta^2\sigma^2(U_j)+\sigma^2(K_{tj})\right]^2}, \tag{B.8}$$

and

$$\frac{\partial \zeta}{\partial \sigma^2(K_{tj})} = \frac{-\alpha_j (\beta U_j - K_{tj})^2}{\left[\beta^2 \sigma^2(U_j) + \sigma^2(K_{tj})\right]^2} . \tag{B.9}$$

First Approximation

If the VOV terms are neglected, a first approximation to the standard deviation can be obtained. Neglecting the VOV terms and substituting Eq. (B.6) and Eq. (B.7) into Eq. (B.5) gives

$$\sigma(\zeta_t) = \left\{ \sum_{j=1}^{J} \left[\frac{2\alpha_j (\beta U_j - K_{tj})}{\beta^2 \sigma^2(U_j) + \sigma^2(K_{tj})} \right]^2 \left[\beta^2 \sigma^2(U_j) + \sigma^2(K_{tj})\right] \right\}^{1/2} . \tag{B.10}$$

Simplifying Eq. (B.10) gives

$$\sigma(\zeta_t) = 2\left[\sum_{j=1}^{J} \alpha_j^2 \frac{(\beta U_j - K_{tj})^2}{\left(\beta^2 \sigma^2(U_j) + \sigma^2(K_{tj})\right)} \right]^{1/2} .$$

This first approximation is the one used in the original formulation of the SBRS technique [3, 4].

Second Approximation

If the VOV terms are not neglected, a second, more accurate approximation to the standard deviation of the figure-of-merit can be made. Using the result derived in Appendix C, the VOV is given by

$$\sigma^2(\sigma^2(x)) = \sigma^2(x) . \tag{B.11}$$

Therefore the VOV of the variance terms can be written as

$$\sigma^2(\sigma^2(U_j)) = \sigma^2(U_j), \tag{B.12}$$

and

$$\sigma^2(\sigma^2(K_{tj})) = \sigma^2(K_{tj}). \tag{B.13}$$

Substituting Eqs. (B.6), (B.7), (B.8), and (B.9) into Eq. (B.5) gives

$$\sigma(\zeta_t) = \left\{ \begin{array}{l} \sum_{j=1}^{J} \left[\frac{\alpha_j (2)\left(\beta U_j - K_{tj}\right)}{\beta^2 \sigma^2(U_j) + \sigma^2(K_{tj})} \right]^2 \left[\beta^2 \sigma^2(U_j) + \sigma^2(K_{tj})\right] \\ + \sum_{j=1}^{J} \left[\frac{\alpha_j \left(\beta U_j - K_{tj}\right)^2}{\left(\beta^2 \sigma^2(U_j) + \sigma^2(K_{tj})\right)^2} \right]^2 \left[\beta^4 \sigma^2(\sigma^2(U_j)) + \sigma^2(\sigma^2(K_{tj}))\right] \end{array} \right\}^{1/2}. \tag{B.14}$$

Simplifying the first term, and rewriting the second term so that they have a common factor gives

$$\sigma(\zeta_t) = \left\{ \begin{array}{l} \sum_{j=1}^{J} \left[\frac{\alpha_j^2 (4)\left(\beta U_j - K_{tj}\right)^2}{\beta^2 \sigma^2(U_j) + \sigma^2(K_{tj})} \right] \\ + \sum_{j=1}^{J} \left[\frac{\alpha_j^2 (4)\left(\beta U_j - K_{tj}\right)^2}{\beta^2 \sigma^2(U_j) + \sigma^2(K_{tj})} \right] \left(\frac{1}{4}\right) \left(\frac{\left(\beta U_j - K_{tj}\right)^2}{\left(\beta^2 \sigma^2(U_j) + \sigma^2(K_{tj})\right)^3} \right) \left[\beta^4 \sigma^2(\sigma^2(U_j)) + \sigma^2(\sigma^2(K_{tj}))\right] \end{array} \right\}^{1/2}$$

Factoring out the common term results in

$$\sigma(\zeta_t) = \left\{ \sum_{j=1}^{J} \left[\frac{\alpha_j^2 (4)\left(\beta U_j - K_{tj}\right)^2}{\beta^2 \sigma^2(U_j) + \sigma^2(K_{tj})} \right] \left[1 + \frac{\left(\beta U_j - K_{tj}\right)^2 \left(\beta^4 \sigma^2(\sigma^2(U_j)) + \sigma^2(\sigma^2(K_{tj}))\right)}{4\left(\beta^2 \sigma^2(U_j) + \sigma^2(K_{tj})\right)^3} \right] \right\}^{1/2}.$$

Substituting the VOV terms by Eqs. (B.12) and (B.13) gives

$$\sigma(\zeta_t)=\left\{\sum_{j=1}^{J}\left[\frac{\alpha_j^2(4)\left(\beta U_j-K_{tj}\right)^2}{\beta^2\sigma^2(U_j)+\sigma^2(K_{tj})}\right]\left[1+\frac{\left(\beta U_j-K_{tj}\right)^2\left(\beta^4\sigma^2(U_j)+\sigma^2(K_{tj})\right)}{4\left(\beta^2\sigma^2(U_j)+\sigma^2(K_{tj})\right)^3}\right]\right\}^{1/2}. \quad \text{(B.15)}$$

The results calculated for each bin of the MCNP5 simulations are given in gammas emitted from the target per incident neutron. Therefore, in order to illustrate the use of the standard deviation of the FOM for a realistic situation, it can be assumed that the the total number of neutrons emitted to the target, times the efficiency of the gamma detector, results in 10^9 counts. The results in Table B.1 are obtained by multiplying the results from each bin used for calculations by 10^9, and by assuming that the counts are poisoned distributed. The figure-of-merit and their corresponding standard deviations (with and without the VOV terms) for two explosive and two inert samples, are compare in Table B.1.

Table B.1 Comparison of FOM Standard Deviation With and Without the VOV Terms

	Z	σ(ζ) without VOV Term	σ(ζ) with VOV Term	Percentage Difference(%)
Aluminum Explosive	8.58	1.95	1.98	1.31
Aluminum Inert	49.99	4.71	5.23	10.36
Salt Explosive	3.73	1.29	1.29	0.53
Salt Inert	50.02	4.71	5.23	10.35

APPENDIX C

This Appendix shows two derivations. First, the derivation of the variance of the sample variance for a Poisson distribution is presented. Then, the VOV for the net peaks of the signatures used in the figure-of-merit is derived.

Starting with the definition of variance, the variance of the sample variance is given by

$$\sigma^2(\hat{\sigma}^2(k)) = E[(\hat{\sigma}^2(k) - \sigma^2)^2), \tag{C.1}$$

where $\sigma^2(k)$ is the sample variance based on k observations and σ^2 is the population variance.

For a poisson distribution, the mean and the variance have the same value. This fact can be used to express the VOV for a poisson distribution in terms of the sample mean, such that

$$\sigma^2 = \mu, \tag{C.2}$$

and

$$\sigma^2(k) = \hat{x}(k) = \frac{1}{k}\sum_{i=1}^{k} x(i), \tag{C.3}$$

where $x(k)$ is the sample mean based on k observations, μ is the population mean, and $x(i)$ is the measurement value for the *ith* observation. Substituting Eqs. (C.2) and (C.3) into Eq. (C.1) gives

$$
\begin{aligned}
\sigma^2(\hat{\sigma}^2(k)) &= E\left[\left(\frac{1}{k}\sum_{i=1}^{k}x(i)-\mu\right)^2\right] \\
&= E\left[\left(\frac{1}{k^2}\left(\sum_{i=1}^{k}x(i)\right)^2-\frac{2\mu}{k}\sum_{i=1}^{k}x(i)+\mu^2\right)\right] \\
&= E\left[\left(\frac{1}{k^2}\sum_{i=1}^{k}x^2(i)+\frac{1}{k^2}\sum_{i=1}^{k}\sum_{j=1}^{k}x(i)x(j)-\frac{2\mu}{k}\sum_{i=1}^{k}x(i)+\mu^2\right)\right] \\
&= \frac{1}{k^2}\sum_{i=1}^{k}E\left[x^2(i)\right]+\frac{1}{k^2}\sum_{i=1}^{k}\sum_{j=1}^{k}E\left[x(i)\right]E\left[x(j)\right]-\frac{2\mu}{k}\sum_{i=1}^{k}E\left[x(i)\right]+E\left[\mu^2\right] \\
&= \left(\frac{1}{k^2}\right)(k)\left\langle x^2\right\rangle+\left(\frac{1}{k^2}\right)(k)(k-1)\left\langle x\right\rangle\left\langle x\right\rangle-\left(\frac{2\mu}{k}\right)(k)\left\langle x\right\rangle+\mu^2
\end{aligned}
.
$$

By realizing that

$$
\left\langle x^2\right\rangle = \sigma^2+\left\langle x\right\rangle^2, \tag{C.4}
$$

and

$$
\left\langle x\right\rangle = \mu, \tag{C.5}
$$

then

$$
\begin{aligned}
\sigma^2(\hat{\sigma}^2(k)) &= \frac{1}{k}\left(\sigma^2+\left\langle x\right\rangle^2\right)+\frac{(k-1)}{k}\left\langle x^2\right\rangle-2\mu\left\langle x\right\rangle+\mu^2 \\
&= \frac{1}{k}\left(\mu+\mu^2\right)+\left(1-\frac{1}{k}\right)\mu^2-2\mu^2+\mu^2 \\
&= \frac{\mu}{k}+\frac{\mu^2}{k}+\mu^2-\frac{\mu^2}{k}-2\mu^2+\mu^2 \\
&= \frac{\mu}{k}
\end{aligned}
. \tag{C.6}
$$

Because μ is not known it should be approximated by the sample mean or the sample variance, such that

$$\sigma^2(\hat{\sigma}^2(k)) = \frac{\hat{x}(k)}{k} = \frac{1}{k^2}\sum_{i=1}^{k} x(i) \quad , \tag{C.7}$$

or in terms of the sample variance is

$$\sigma^2(\hat{\sigma}^2(k)) = \frac{\hat{\sigma}^2(k)}{k} \quad . \tag{C.8}$$

Now, the variance of the sample variance for the signatures used in the figure-of-merit is derived. The net peak of a signature obtained from an unknown target is given by

$$R_{no} = R_n - \frac{(R_{n+1} - R_{n-1})}{2} \tag{C.9}$$

where R_n, is the number of counts for the n^{th} bin, and R_{n+1}, and R_{n-1} are the number of counts for the two adjacent bins. Applying the standard propagation of errors formula to Eq. (C.9) gives

$$\begin{aligned} \sigma(R_{no}) &= \left[\sigma^2(R_n) + \left(\frac{1}{2}\right)^2 \left[\sigma^2(R_{n+1}) + \sigma^2(R_{n-1})\right] \right]^{1/2} \\ &= \left[\sigma^2(R_n) + \frac{1}{4}\sigma^2(R_{n+1}) + \frac{1}{4}\sigma^2(R_{n-1}) \right]^{1/2} \quad . \end{aligned} \tag{C.10}$$

Therefore

$$\sigma^2(R_{no}) = \sigma^2(R_n) + \frac{1}{4}\sigma^2(R_{n+1}) + \frac{1}{4}\sigma^2(R_{n-1}) \quad . \tag{C.12}$$

By applying the standard propagation of errors formula again to Eq. (C.12) it follows that

$$\sigma\left(\sigma^2\left(R_{no}\right)\right)=\left[\sigma^2\left(\sigma^2\left(R_n\right)\right)+\frac{1}{4}\sigma^2\left(\sigma^2\left(R_{n+1}\right)\right)+\frac{1}{4}\sigma^2\left(\sigma^2\left(R_{n-1}\right)\right)\right]^{1/2}. \tag{C.13}$$

Assuming a poisson distribution for the counts under each bin and using Eq. (C.8) with *k=1* yields

$$\begin{aligned}\sigma\left(\sigma^2\left(R_{no}\right)\right)&=\left[\sigma^2\left(R_n\right)+\frac{1}{4}\sigma^2\left(R_{n+1}\right)+\frac{1}{4}\sigma^2\left(R_{n-1}\right)\right]^{1/2}\\&=\sigma\left(R_{no}\right)\end{aligned}. \tag{C.14}$$

Therefore, the variance of the sample variance for the net peak of a signature is given by

$$\sigma^2\left(\sigma^2\left(R_{no}\right)\right)=\sigma^2\left(R_{no}\right). \tag{C.15}$$

APPENDIX D1

This Appendix shows the cut-off values for each tier of the tiered-filter approach and the cut-off value for the non-tiered approach, as well as the False Negatives and False Positives of the results for both methods shown in section 5.4. In the Table, the values under the title range indicate the range of values that the cutoff could have taken and still obtain the same result.

Table D1.1. Cut-Off Values for Results Using the Tiered Approach on Samples with the Same Geometrical Configuration as the Default Configuration

	Lower Density Tier			Higher Density Tier		
	Cut-Off	Range		Cut-Off	Range	
H	16	16	40	5	0	5
C	62	62	125	44	44	90
N	58	58	78	144	144	178
O	24	24	29	84	50	84

Table D1.2. Cut-Off Values for Results Using the Non-Tiered Approach on Samples with the Same Geometrical Configuration as the Default Configuration

	Lower Density Tier	Higher Density Tier
Cut-Off	**4**	**49**

Table D1.3. False Positives and False Negatives for Results Using the Tiered Approach on Samples with the Same Geometrical Configuration as the Default Configuration

	Lower Density Tier		Higher Density Tier	
	False Positive	False Negative	False Positive	False Negative
1	Fertilizer A	Aluminum		Titanium
2	Fertilizer B			
3	Nylon			

Table D1.4. False Positives and False Negatives for Results Using the Non-Tiered Approach on Samples with the Same Geometrical Configuration as the Default Configuration

	Lower Density Tier		Higher Density Tier	
	False Positive	False Negative	False Positives	False Negatives
1	Fertilizer A	Herbicide 2		
2	Herbicide 1			
3	Nylon			
4	Tissue			
5	Water			

APPENDIX D2

This Appendix shows the cut-off values for each tier of the tiered-filter approach and the cut-off value for the non-tiered approach, as well as the False Negatives and False Positives of the results for both methods shown in section 5.5. In the Table, the values under the title range indicate the range of values that the cutoff could have taken and still obtain the same result.

Table D2.1. Cut-Off Values for Results Using the Tiered Approach
On Samples 10 cm Closer to the Source than the Default Configuration

	Lower Density Tier			Higher Density Tier		
	Cut-Off	Range		Cut-Off	Range	
H	85	80	85	0	0	1
C	50	11	50	200	200	200
N	71	71	89	200	200	200
O	29	13	29	71	56	96

Table D2.2. Cut-Off Values for Results Using the Non-Tiered Approach
On Samples 10 cm Closer to the Source than the Default Configuration

	Lower Density Tier	Higher Density Tier
Cut-Off	**4**	**49**

Table D2.3. False Positives and False Negatives for Results Using the Tiered Approach On Samples 10 cm Closer to the Source than the Default Configuration

	Lower Density Tier		Higher Density Tier	
	False Positive	False Negative	False Positive	False Negative
1	Fertilizer A	Aluminum		Titanium
2	Herbicide 1			
3	Nylon			

Table D2.4. False Positives and False Negatives for Results Using the Non-Tiered Approach On Samples 10 cm Closer to the Source than the Default Configuration

	Lower Density Tier		Higher Density Tier	
	False Positive	False Negative	False Positives	False Negatives
1	Antifreeze	Fertilizer A		
2	Cotton			
3	Fertilizer A			
4	Herbicide 1			
5	Limestone			
6	Lucite			
7	Nylon			
8	Plexiglass			
9	Tissue			
10	Water			

Table D2.5. Cut-Off Values for Results Using the Tiered Approach On Samples 20 cm Closer to the Source than the Default Configuration

	Lower Density Tier			Higher Density Tier		
	Cut-Off	Range		Cut-Off	Range	
H	25	25	34	172	161	178
C	117	117	147	199	200	200
N	69	69	74	111	55	111
O	21	21	23	39	37	39

Table D2.6. Cut-Off Values for Results Using the Non-Tiered Approach
On Samples 20 cm Closer to the Source than the Default Configuration

	Lower Density Tier	Higher Density Tier
Cut-Off	**6**	**41**

Table D2.7. False Positives and False Negatives for Results Using the Tiered Approach
On Samples 20 cm Closer to the Source than the Default Configuration

	Lower Density Tier		Higher Density Tier	
	False Positive	False Negative	False Positive	False Negative
1	Fertilizer A	Aluminum		
2	Herbicide 1	Concrete		
3	Nylon			

Table D2.8. False Positives and False Negatives for Results Using the Non-Tiered Approach
On Samples 20 cm Closer to the Source than the Default Configuration

	Lower Density Tier		Higher Density Tier	
	False Positive	False Negative	False Positives	False Negatives
1	Antifreeze	Carbon		
2	Ethanol	Cardboard		
3	Herbicide 1	Cherrywood		
4	Limestone	Fertilizer A		
5	Lucite	Polyurethane		
6	Nylon	Tissue		
7	Petroleum	Water		
8	Plexiglass	Woodoak		
9	Polyethylene			
10	Sugar			
11	Tissue			
12	Wax			

Table D2.9. Cut-Off Values for Results Using the Tiered Approach on Samples from the Default Configuration as well as Samples 10 cm and 20 cm Closer to the Source

	Lower Density Tier			Higher Density Tier		
	Cut-Off	Range		Cut-Off	Range	
H	24	24	33	138	137	200
C	181	181	191	200	199	200
N	65	65	75	200	195	200
O	27	27	29	67	41	79

Table D2.10. Cut-Off Values for Results Using the Non-Tiered Approach on Samples from the Default Configuration as well as Samples 10 cm and 20 cm Closer to the Source

	Lower Density Tier	Higher Density Tier
Cut-Off	**4**	**50**

Table D2.11. False Positives and False Negatives for Results Using the Tiered Approach on Samples from the Default Configuration as well as Samples 10 cm and 20 cm Closer to the Source

	Lower Density Tier				Higher Density Tier			
	False Positive		False Negative		False Positive		False Negative	
1	Fertilizer A		Aluminum					
2	Herbicide 1		Concrete					
3	Nylon		Aluminum					
4	Fertilizer A		Aluminum					
5	Herbicide 1							
6	Nylon							
7	Fertilizer A							
8	Herbicide 1							
9	Nylon							

Table D2.12. False Positives and False Negatives for Results Using the Non-Tiered Approach on Samples from the Default Configuration as well as Samples 10 cm and 20 cm Closer to the Source

	Lower Density Tier				Higher Density Tier			
	False Positive		False Negative		False Positives		False Negatives	
1	Fertilizer A		Herbicide 2					
2	Herbicide 1		Fertilizer A					
3	Nylon		Air					
4	Tissue		Antifreeze					
5	Water		Carbon					
6	Antifreeze		Cardboard					
7	Cotton		Cherrywood					
8	Fertilizer A		Cotton					
9	Herbicide 1		Cyanurate					
10	Limestone		Fertilizer A					
11	Lucite		Petroleum					
12	Nylon		Polyethylene					
13	Plexiglass		Polypropylene					
14	Tissue		Polystyrene					
15	Water		Polyurethane					
16	Antifreeze		Propane					
17	Ethanol		Rubber					
18	Herbicide 1		Styrafoam					
19	Petroleum		Sugar					
20	Tissue		Tissue					
21	Wax		Void					
22			Water					
23			Wax					
24			Woodoak					

APPENDIX D3

This Appendix shows the cut-off values for each tier of the tiered-filter approach and the cut-off value for the non-tiered approach, as well as the False Negatives and False Positives of the results for both methods shown in section 5.6. In the Table, the values under the title range indicate the range of values that the cutoff could have taken and still obtain the same result.

Table D3.1. Cut-Off Values for Results Using the Tiered Approach on Samples with Explosive 5 cm Thicker than the Default Configuration

	Lower Density Tier			Higher Density Tier		
	Cut-Off	Range		Cut-Off	Range	
H	72	72	97	64	60	72
C	25	25	47	195	196	197
N	34	34	55	53	53	79
O	7	7	21	155	123	155

Table D3.2. Cut-Off Values for Results Using the Non-Tiered Approach on Samples with Explosive 5 cm Thicker than the Default Configuration

	Lower Density Tier	Higher Density Tier
Cut-Off	**5**	**90**

Table D3.3. False Positives and False Negatives for Results Using the Tiered Approach on Samples with Explosive 5 cm Thicker than the Default Configuration

	Lower Density Tier		Higher Density Tier	
	False Positive	False Negative	False Positive	False Negative
1	Fertilizer A			
2	Herbicide 1			
3	Nylon			

Table D3.4. False Positives and False Negatives for Results Using the Non-Tiered Approach on Samples with Explosive 5 cm Thicker than the Default Configuration

	Lower Density Tier		Higher Density Tier	
	False Positive	False Negative	False Positives	False Negatives
1	Antifreeze	Fertilizer A	Steel	
2	Cotton			
3	Fertilizer A			
4	Herbicide 1			
5	Limestone			
6	Lucite			
7	Nylon			
8	Plexiglass			
9	Tissue			
10	Water			

Table D3.5. Cut-Off Values for Results Using the Tiered Approach on Samples with Explosive 10 cm Thicker than the Default Configuration

	Lower Density Tier			Higher Density Tier		
	Cut-Off	Range		Cut-Off	Range	
H	81	81	87	14	2	14
C	51	51	53	200	200	200
N	18	18	18	130	129	175
O	46	46	49	21	11	36

Table D3.6. Cut-Off Values for Results Using the Non-Tiered Approach on Samples with Explosive 10 cm Thicker than the Default Configuration

	Lower Density Tier	Higher Density Tier
Cut-Off	**6**	**86**

Table D3.7. False Positives and False Negatives for Results Using the Tiered Approach on Samples with Explosive 10 cm Thicker than the Default Configuration

	Lower Density Tier		Higher Density Tier	
	False Positive	False Negative	False Positive	False Negative
1	Fertilizer A			Titanium
2	Herbicide 1			Zirconium
3	Nylon			
4	Petroleum			

Table D3.8. False Positives and False Negatives for Results Using the Non-Tiered Approach on Samples with Explosive 10 cm Thicker than the Default Configuration

	Lower Density Tier		Higher Density Tier	
	False Positive	False Negative	False Positives	False Negatives
1	Antifreeze	Fertilizer A	Steel	
2	Cotton			
3	Ethanol			
4	Fertilizer A			
5	Herbicide 1			
6	Limestone			
7	Lucite			
8	Nylon			
9	Petroleum			
10	Plexiglass			
11	Sugar			
12	Tissue			
13	Water			

Table D3.9. Cut-Off Values for Results Using the Tiered Approach on Samples with Explosive 15 cm Thicker than the Default Configuration

	Lower Density Tier			Higher Density Tier		
	Cut-Off	Range		Cut-Off	Range	
H	92	92	95	199	198	200
C	84	84	94	160	139	184
N	46	46	63	45	45	86
O	24	24	24	120	47	200

Table D3.10. Cut-Off Values for Results Using the Non-Tiered Approach on Samples with Explosive 15 cm Thicker than the Default Configuration

	Lower Density Tier	Higher Density Tier
Cut-Off	**6**	**60**

Table D3.11. False Positives and False Negatives for Results Using the Tiered Approach on Samples with Explosive 15 cm Thicker than the Default Configuration

	Lower Density Tier		Higher Density Tier	
	False Positive	False Negative	False Positive	False Negative
1	Fertilizer A			Zirconium
2	Herbicide 1			
3	Nylon			

Table D3.12. False Positives and False Negatives for Results Using the Non-Tiered Approach on Samples with Explosive 15 cm Thicker than the Default Configuration

	Lower Density Tier		Higher Density Tier	
	False Positive	False Negative	False Positives	False Negatives
1	Antifreeze	Air		
2	Cotton	Antifreeze		
3	Ethanol	Cardboard		
4	Herbicide 1	Cherrywood		
5	Limestone	Cyanurate		
6	Lucite	Fertilizer A		
7	Nylon	Polystyrene		
8	Petroleum	Polyurethane		
9	Plexiglass	Propane		
10	Sugar	Tissue		
11	Tissue	Void		
12	Wax	Water		
13		Woodoak		

Table D3.13. Cut-Off Values for Results Using the Tiered Approach on Samples from the Default Configuration as well as with Explosives 5, 10 and 15 cm Thicker

	Lower Density Tier			Higher Density Tier		
	Cut-Off	Range		Cut-Off	Range	
H	95	90	97	0	0	1
C	180	168	193	200	159	200
N	50	50	62	192	193	196
O	17	17	24	75	75	86

Table D3.14. Cut-Off Values for Results Using the Non-Tiered Approach on Samples from the Default Configuration as well as with Explosives 5, 10 and 15 cm Thicker

	Lower Density Tier	Higher Density Tier
Cut-Off	**6**	**49**

Table D3.15. False Positives and False Negatives for Results Using the Tiered Approach on Samples from the Default Configuration as well as with Explosives 5, 10 and 15 cm Thicker

	Lower Density Tier		Higher Density Tier	
	False Positive	False Negative	False Positive	False Negative
1	Fertilizer A	Aluminum		Titanium
2	Herbicide 1			Titanium
3	Nylon			Titanium
4	Fertilizer A			Zirconium
5	Herbicide 1			Titanium
6	Nylon			Zirconium
7	Fertilizer A			
8	Herbicide 1			
9	Nylon			
10	Fertilizer A			
11	Herbicide 1			
12	Nylon			

Table D3.16. Cut-Off Values for Results Using the Non-Tiered Approach on Samples from the Default Configuration as well as with Explosives 5, 10 and 15 cm Thicker

	Lower Density Tier		Higher Density Tier	
	False Positive	False Negative	False Positives	False Negatives
1	Antifreeze	Fertilizer A		
2	Cotton	Air		
3	Fertilizer A	Antifreeze		
4	Herbicide 1	Cardboard		
5	Limestone	Cherrywood		
6	Lucite	Cyanurate		
7	Nylon	Fertilizer A		
8	Plexiglass	Polystyrene		
9	Sugar	Polyurethane		
10	Tissue	Propane		
11	Water	Tissue		
12	Antifreeze	Void		

Table D3.16. Cut-Off Values for Results Using the Non-Tiered Approach on Samples from the Default Configuration as well as with Explosives 5, 10 and 15 cm Thicker

	Lower Density Tier				Higher Density Tier			
	False Positive		False Negative		False Positives		False Negatives	
13	Cotton		Water					
14	Ethanol		Woodoak					
15	Fertilizer A							
16	Herbicide 1							
17	Limestone							
18	Lucite							
19	Nylon							
20	Plexiglass							
21	Sugar							
22	Tissue							
23	Water							
24	Antifreeze							
25	Cotton							
26	Ethanol							
27	Fertilizer A							
28	Herbicide 1							
29	Limestone							
30	Lucite							
31	Nylon							
32	Petroleum							
33	Plexiglass							
34	Sugar							
35	Tissue							
36	Water							
37	Antifreeze							
38	Cotton							
39	Ethanol							
40	Herbicide 1							
41	Limestone							
42	Lucite							
43	Nylon							

Table D3.16. Cut-Off Values for Results Using the Non-Tiered Approach on Samples from the Default Configuration as well as with Explosives 5, 10 and 15 cm Thicker

	Lower Density Tier			Higher Density Tier			
	False Positive		False Negative	False Positives		False Negatives	
44	Petroleum						
45	Plexiglass						
46	Sugar						
47	Tissue						
48	Wax						

APPENDIX D4

This Appendix shows the cut-off values for each tier of the tiered-filter approach and the cut-off value for the non-tiered approach, as well as the False Negatives and False Positives of the results for both methods shown in section 5.7. In the Table, the values under the title range indicate the range of values that the cutoff could have taken and still obtain the same result.

Table D4.1. Cut-Off Values for Results Using the Tiered Approach on Samples with Clutter 5 cm Thicker than the Default Configuration

	Lower Density Tier			Higher Density Tier		
	Cut-Off	Range		Cut-Off	Range	
H	101	101	104	4	4	17
C	31	31	48	168	75	168
N	54	54	62	73	74	97
O	26	26	27	200	164	200

Table D4.2. Cut-Off Values for Results Using the Non-Tiered Approach on Samples with Clutter 5 cm Thicker than the Default Configuration

	Lower Density Tier	Higher Density Tier
Cut-Off	**7**	**86**

Table D4.3. False Positives and False Negatives for Results Using the Tiered Approach on Samples with Clutter 5 cm Thicker than the Default Configuration

	Lower Density Tier		Higher Density Tier	
	False Positive	False Negative	False Positive	False Negative
1	Fertilizer A			
2	Herbicide 1			
3	Nylon			
4	Polyurethane			
5	Tissue			

Table D4.4. False Positives and False Negatives for Results Using the Non-Tiered Approach on Samples with Clutter 5 cm Thicker than the Default Configuration

	Lower Density Tier		Higher Density Tier	
	False Positive	False Negative	False Positives	False Negatives
1	Antifreeze	Aluminum	Steel	
2	Cotton	Salt		
3	Ethanol			
4	Fertilizer A			
5	Herbicide 1			
6	Limestone			
7	Lucite			
8	Nylon			
9	Petroleum			
10	Glass			
11	Sugar			
12	Tissue			
13	Wax			

Table D4.5. Cut-Off Values for Results Using the Tiered Approach on Samples with Clutter 10 cm Thicker than the Default Configuration

	Lower Density Tier			Higher Density Tier		
	Cut-Off	Range		Cut-Off	Range	
H	125	125	127	0	0	1
C	30	30	73	176	168	193
N	24	24	28	170	163	191
O	26	26	27	60	60	87

Table D4.6. Cut-Off Values for Results Using the Non-Tiered Approach on Samples with Clutter 10 cm Thicker than the Default Configuration

	Lower Density Tier	Higher Density Tier
Cut-Off	**3**	**86**

Table D4.7. False Positives and False Negatives for Results Using the Tiered Approach on Samples with Clutter 10 cm Thicker than the Default Configuration

	Lower Density Tier		Higher Density Tier	
	False Positive	False Negative	False Positive	False Negative
1	Fertilizer A	Aluminum		
2	Herbicide 1	Glass		
3	Nylon			
4	Polyurethane			
5	Tissue			

Table D4.8. False Positives and False Negatives for Results Using the Non-Tiered Approach on Samples with Clutter 10 cm Thicker than the Default Configuration

	Lower Density Tier		Higher Density Tier	
	False Positive	False Negative	False Positives	False Negatives
1	Ethanol	Aluminum	Steel	
2	Herbicide 1	Borax		
3	Tissue	Carbon		
4		Ceramic		
5		Concrete		
6		Fertilizer A		
7		Glass		
8		Granite		
9		Herbicide 3		
10		Khydroxide		
11		Nylon		
12		Salt		
13		Soap		
14		Soil		
15		Soy		
16		Styrafoam		
17		Water		
18		Woodoak		

Table D4.9. Cut-Off Values for Results Using the Tiered Approach on Samples with Clutter 15 cm Thicker than the Default Configuration

	Lower Density Tier			Higher Density Tier		
	Cut-Off	Range		Cut-Off	Range	
H	169	117	169	0	0	1
C	64	52	64	67	64	67
N	55	55	58	199	199	200
O	47	47	48	83	80	87

Table D4.10. Cut-Off Values for Results Using the Non-Tiered Approach on Samples with Clutter 15 cm Thicker than the Default Configuration

	Lower Density Tier	Higher Density Tier
Cut-Off	**4**	**85**

Table D4.11. False Positives and False Negatives for Results Using the Tiered Approach on Samples with Clutter 15 cm Thicker than the Default Configuration

	Lower Density Tier		Higher Density Tier	
	False Positive	False Negative	False Positive	False Negative
1	Fertilizer A			
2	Herbicide 1			
3	Nylon			
4	Petroleum			
5	Polyurethane			
6	Tissue			

Table D4.12. False Positives and False Negatives for Results Using the Non-Tiered Approach on Samples with Clutter 15 cm Thicker than the Default Configuration

	Lower Density Tier		Higher Density Tier	
	False Positive	False Negative	False Positives	False Negatives
1	Antifreeze	Aluminum	Steel	
2	Ethanol	Borax		
3	Herbicide 1	Carbon		
4	Petroleum	Cardboard		
5	Polyethylene	Ceramic		
6	Polypropylene	Cotton		
7	Tissue	Fertilizer A		
8		Glass		
9		Granite		
10		Herbicide 2		
11		Herbicide 3		
12		Khydroxide		
13		Lucite		
14		Nylon		
15		Salt		
16		Soap		
17		Soil		
18		Sugar		
19		Woodoak		

Table D4.13. Cut-Off Values for Results Using the Tiered Approach on Samples with Clutter 20 cm Thicker than the Default Configuration

	Lower Density Tier			Higher Density Tier		
	Cut-Off	Range		Cut-Off	Range	
H	80	80	96	0	0	1
C	52	52	68	77	75	99
N	84	84	91	200	197	200
O	60	60	67	200	195	200

Table D4.14. Cut-Off Values for Results Using the Non-Tiered Approach on Samples with Clutter 20 cm Thicker than the Default Configuration

	Lower Density Tier	Higher Density Tier
Cut-Off	**5**	**79**

Table D4.15. False Positives and False Negatives for Results Using the Tiered Approach on Samples with Clutter 20 cm Thicker than the Default Configuration

	Lower Density Tier		Higher Density Tier	
	False Positive	False Negative	False Positive	False Negative
1	Fertilizer A	Aluminum	Steel	
2	Herbicide 1	Bricks		
3	Nylon	Cermic		
4	Petroleum	Concrete		
5	Tissue	Glass		
6		Granite		
7		Salt		

Table D4.16. False Positives and False Negatives for Results Using the Non-Tiered Approach on Samples with Clutter 20 cm Thicker than the Default Configuration

	Lower Density Tier		Higher Density Tier	
	False Positive	False Negative	False Positives	False Negatives
1	Ethanol	Aluminum	Steel	
2	Gasoline	Borax		
3	Petroleum	Carbon		
4	Soap	Cardboard		
5	Tissue	Ceramic		
6		Cotton		
7		Fertilizer A		
8		Glass		
9		Granite		
10		Herbicide 1		
11		Herbicide 2		
12		Herbicide 3		
13		Khydroxide		
14		Limestone		
15		Lucite		
16		Nylon		
17		Plexiglass		
18		Salt		
19		Soil		
20		Soy		
21		Sugar		
22		Woodoak		

Table D4.17. Cut-Off Values for Results Using the Tiered Approach on Samples from the Default Configuration as well as with Clutter 5, 10, 15 and 20 cm Thicker

	Lower Density Tier			Higher Density Tier		
	Cut-Off	Range		Cut-Off	Range	
H	172	172	172	0	0	1
C	45	45	46	75	76	89
N	61	61	61	185	185	195
O	22	22	22	95	94	99

Table D4.18. Cut-Off Values for Results Using the Non-Tiered Approach on Samples from the Default Configuration as well as with Clutter 5, 10, 15 and 20 cm Thicker

	Lower Density Tier	Higher Density Tier
Cut-Off	**5**	**78**

Table D4.19. False Positives and False Negatives for Results Using the Tiered Approach on Samples from the Default Configuration as well as with Clutter 5, 10, 15 and 20 cm Thicker

	Lower Density Tier		Higher Density Tier	
	False Positive	False Negative	False Positive	False Negative
1	Herbicide 1	Aluminum		Steel
2	Nylon	Carbon		Titanium
3	Petroleum	Fertilizer A		
4	Polyurethane	Salt		
5	Tissue	Aluminum		
6	Fertilizer A	Salt		
7	Herbicide 1	Aluminum		
8	Nylon	Salt		
9	Polyurethane			
10	Tissue			
11	Fertilizer A			
12	Herbicide 1			
13	Nylon			
14	Polyurethane			
15	Tissue			
16	Bricks			
17	Herbicide 1			
18	Nylon			
19	Polyurethane			
20	Tissue			
21	Fertilizer A			
22	Herbicide 1			
23	Nylon			
24	Polyurethane			
25	Tissue			

Table D4.20. False Positives and False Negatives for Results Using the Non-Tiered Approach on Samples from the Default Configuration as well as with Clutter 5, 10, 15 and 20 cm Thicker

	Lower Density Tier		Higher Density Tier			
	False Positive	False Negative	False Positives		False Negatives	
1	Antifreeze	Aluminum	Steel			
2	Cotton	Fertilizer A	Steel			
3	Fertilizer A	Khydroxide	Steel			
4	Herbicide 1	Salt	Steel			
5	Limestone	Aluminum	Steel			
6	Lucite	Fertilizer A				
7	Nylon	Herbicide 3				
8	Plexiglass	Salt				
9	Sugar	Soil				
10	Tissue	Water				
11	Water	Khydroxide				
12	Antifreeze	Woodoak				
13	Cotton	Aluminum				
14	Ethanol	Borax				
15	Fertilizer A	Carbon				
16	Herbicide 1	Cardboard				
17	Limestone	Ceramic				
18	Lucite	Fertilizer A				
19	Nylon	Glass				
20	Petroleum	Granite				
21	Glass	Herbicide 2				
22	Sugar	Herbicide 3				
23	Tissue	Khydroxide				
24	Antifreeze	Nylon				
25	Cotton	Salt				
26	Ethanol	Soil				
27	Fertilizer A	Woodoak				
28	Herbicide 1	Aluminum				
29	Herbicide 2	Borax				
30	Limestone	Carbon				
31	Lucite	Cardboard				

Table D4.20. False Positives and False Negatives for Results Using the Non-Tiered Approach on Samples from the Default Configuration as well as with Clutter 5, 10, 15 and 20 cm Thicker

	Lower Density Tier				Higher Density Tier			
	False Positive		False Negative		False Positives		False Negatives	
32	Nylon		Ceramic					
33	Petroleum		Cotton					
34	Plexiglass		Fertilizer A					
35	Polyethylene		Glass					
36	Polypropylene		Granite					
37	Soy		Herbicide 1					
38	Sugar		Herbicide 2					
39	Tissue		Herbicide 3					
40	Antifreeze		Khydroxide					
41	Ethanol		Limestone					
42	Herbicide 1		Lucite					
43	Petroleum		Nylon					
44	Polyethylene		Plexiglass					
45	Polypropylene		Salt					
46	Tissue		Soil					
47	Ethanol		Soy					
48	Gasoline		Sugar					
49	Petroleum		Woodoak					
50	Soap							
51	Tissue							

APPENDIX D5

This Appendix shows the cut-off values for each tier of the tiered-filter approach and the cut-off value for the non-tiered approach, as well as the False Negatives and False Positives of the results for both methods shown in section 5.8. In the Table, the values under the title range indicate the range of values that the cutoff could have taken and still obtain the same result.

Table D5.1. Cut-Off Values for Results Using the Tiered Approach on All Samples Generated for this Study

	Lower Density Tier			Higher Density Tier		
	Cut-Off	Range		Cut-Off	Range	
H	106	106	109	0	0	1
C	50	50	56	199	199	200
N	61	61	61	198	198	200
O	22	22	22	80	79	86

Table D5.2. Cut-Off Values for Results Using the Non-Tiered Approach on All Samples Generated for this Study

	Lower Density Tier	Higher Density Tier
Cut-Off	**6**	**55**

Table D5.3. False Positives and False Negatives for Results Using the Tiered Approach on All Samples Generated for this Study

	Lower Density Tier		Higher Density Tier	
	False Positive	False Negative	False Positive	False Negative
1	Fertilizer A	Aluminum		Copper
2	Herbicide 1	Carbon		Steel
3	Nylon	Fertilizer A		Titanium
4	Polyurethane	Salt		Titanium
5	Tissue	Aluminum		Titanium
6	Herbicide 1	Salt		Zirconium
7	Nylon	Aluminum		Titanium
8	Petroleum	Salt		Zirconium
9	Polyurethane			Titanium
10	Tissue			Zirconium
11	Fertilizer A			Titanium
12	Herbicide 1			
13	Nylon			
14	Polyurethane			
15	Tissue			
16	Fertilizer A			
17	Herbicide 1			
18	Nylon			
19	Polyurethane			
20	Tissue			
21	Fertilizer A			
22	Herbicide 1			
23	Nylon			
24	Polyurethane			
25	Tissue			

Table D5.3. False Positives and False Negatives for Results Using the Tiered Approach on All Samples Generated for this Study

	Lower Density Tier				Higher Density Tier			
	False Positive		False Negative		False Positive		False Negative	
26	Fertilizer A							
27	Herbicide 1							
28	Nylon							
29	Polyurethane							
30	Tissue							
31	Fertilizer A							
32	Herbicide 1							
33	Nylon							
34	Polyurethane							
35	Tissue							
36	Fertilizer A							
37	Herbicide 1							
38	Nylon							
39	Polyurethane							
40	Tissue							
41	Fertilizer A							
42	Herbicide 1							
43	Nylon							
44	Petroleum							
45	Polyurethane							
46	Tissue							
47	Fertilizer A							
48	Herbicide 1							
49	Nylon							
50	Polyurethane							
51	Tissue							

Table D5.4. False Positives and False Negatives for Results Using the Non-Tiered Approach on All Samples Generated for this Study

	Lower Density Tier		Higher Density Tier	
	False Positive	False Negative	False Positives	False Negatives
1	Antifreeze	Aluminum	Steel	Copper
2	Cotton	Borax	Steel	Lead
3	Fertilizer A	Carbon		Steel
4	Herbicide 1	Cardboard		Zirconium
5	Limestone	Ceramic		Lead
6	Lucite	Cotton		
7	Nylon	Fertilizer A		
8	Plexiglass	Glass		
9	Sugar	Granite		
10	Tissue	Herbicide 1		
11	Water	Herbicide 2		
12	Antifreeze	Herbicide 3		
13	Ethanol	Khydroxide		
14	Gasoline	Lucite		
15	Nylon	Salt		
16	Petroleum	Soil		
17	Polypropylene	Sugar		
18	Rubber	Woodoak		
19	Soap	Aluminum		
20	Tissue	Borax		
21	Water	Carbon		
22	Antifreeze	Cardboard		
23	Ethanol	Fertilizer A		
24	Gasoline	Herbicide 2		
25	Herbicide 1	Herbicide 3		
26	Limestone	Khydroxide		
27	Petroleum	Nylon		
28	Plexiglass	Salt		
29	Polyethylene	Soil		
30	Polypropylene	Woodoak		
31	Rubber	Aluminum		

Table D5.4. False Positives and False Negatives for Results Using the Non-Tiered Approach on All Samples Generated for this Study

	Lower Density Tier				Higher Density Tier			
	False Positive		False Negative		False Positives		False Negatives	
32	Soap		Fertilizer A					
33	Soy		Herbicide 3					
34	Tissue		Salt					
35	Water		Soil					
36	Wax		Water					
37	Antifreeze		Aluminum					
38	Cotton		Khydroxide					
39	Ethanol		Salt					
40	Fertilizer A		Fertilizer A					
41	Herbicide 1		Air					
42	Herbicide 2		Antifreeze					
43	Limestone		Cardboard					
44	Lucite		Cherrywood					
45	Nylon		Cyanurate					
46	Petroleum		Fertilizer A					
47	Plexiglass		Polystyrene					
48	Polyethylene		Polyurethane					
49	Polypropylene		Propane					
50	Soy		Tissue					
51	Sugar		Void					
52	Tissue		Water					
53	Wax		Woodoak					
54	Antifreeze		Carbon					
55	Cotton		Cardboard					
56	Ethanol		Cherrywood					
57	Fertilizer A		Fertilizer A					
58	Herbicide 1		Polyurethane					
59	Limestone		Tissue					
60	Lucite		Water					
61	Nylon		Woodoak					
62	Petroleum		Fertilizer A					

Table D5.4. False Positives and False Negatives for Results Using the Non-Tiered Approach on All Samples Generated for this Study

	Lower Density Tier				Higher Density Tier			
	False Positive		False Negative		False Positives		False Negatives	
63	Plexiglass							
64	Sugar							
65	Tissue							
66	Antifreeze							
67	Cotton							
68	Ethanol							
69	Fertilizer A							
70	Herbicide 1							
71	Limestone							
72	Lucite							
73	Nylon							
74	Plexiglass							
75	Sugar							
76	Tissue							
77	Water							
78	Antifreeze							
79	Cotton							
80	Ethanol							
81	Fertilizer A							
82	Herbicide 1							
83	Lucite							
84	Nylon							
85	Petroleum							
86	Plexiglass							
87	Sugar							
88	Tissue							
89	Water							
90	Antifreeze							
91	Cotton							
92	Ethanol							
93	Herbicide 1							

Table D5.4. False Positives and False Negatives for Results Using the Non-Tiered Approach on All Samples Generated for this Study

	Lower Density Tier				Higher Density Tier			
	False Positive		False Negative		False Positives		False Negatives	
94	Limestone							
95	Lucite							
96	Nylon							
97	Petroleum							
98	Plexiglass							
99	Sugar							
100	Tissue							
101	Wax							
102	Antifreeze							
103	Ethanol							
104	Herbicide 1							
105	Limestone							
106	Lucite							
107	Nylon							
108	Petroleum							
109	Plexiglass							
110	Polyethylene							
111	Sugar							
112	Tissue							
113	Wax							
114	Antifreeze							
115	Cotton							
116	Ethanol							
117	Fertilizer A							
118	Herbicide 1							
119	Limestone							
120	Lucite							
121	Nylon							
122	Plexiglass							
123	Sugar							
124	Tissue							
125	Water							

APPENDIX E

The element involved, the energy (MeV), the type of reaction, and the cross section for each of the nine signatures used in this study are presented in Table E.1.

Table E.1. Properties of Signatures used in the Present Study

Element	Energy (MeV)	Type of Reaction	Thermal σ (barns)	14.1 MeV σ (barns)
Hydrogen	2.2232	Prompt-Capture	0.3326	-
Carbon	4.4390	Inelastic-Scatter	-	0.2106
Nitrogen	2.3128	Inelastic-Scatter	-	0.0557
Nitrogen	3.3786	Inelastic-Scatter	-	0.0109
Nitrogen	4.9151	Inelastic-Scatter	-	0.00687
Nitrogen	5.1059	Inelastic-Scatter	-	0.0437
Nitrogen	6.4462	Inelastic-Scatter	-	0.0122
Oxygen	6.1299	Inelastic-Scatter	-	0.144
Oxygen	6.9171	Inelastic-Scatter	-	0.0317